Listvenite formation during mass transfer into the leading edge of the mantle wedge: Initial results from Oman Drilling Project Hole BT1B

Peter Kelemen, Juan Carlos de Obeso, James Leong, Marguerite Godard, Keishi Okazaki, Alissa Kotowski, Craig Manning, Eric Ellison, Manuel Menzel, Janos Urai, et al.

Listvenite formation during mass transfer into the leading edge of the mantle wedge: Initial results from Oman Drilling Project Hole BT1B

Peter B. Kelemen[1], Juan Carlos de Obeso[2], James A. Leong[1], Marguerite Godard[3], Keishi Okazaki[4], Alissa J. Kotowski[5], Craig E. Manning[6], Eric T. Ellison[7], Manuel D. Menzel[8], Janos L. Urai[8], Greg Hirth[9], Matthew Rioux[10], Daniel F. Stockli[11], Romain Lafay[3], Andreas M. Beinlich[12], Jude A. Coggon[13], Nehal H. Warsi[14], Jürg M. Matter[13], Damon A.H. Teagle[13], Michelle Harris[15], Katsuyoshi Michibayashi[16], Eiichi Takazawa[17], Zaher Al Sulaimani[18] and the Oman Drilling Project Science Team

1: Lamont Doherty Earth Observatory, Columbia University, Palisades NY 10964, peterk@LDEO.columbia.edu 2: Dept. of Geosciences, University of Calgary 3: Géosciences Montpellier, Université de Montpellier, CNRS 4: Kochi Institute for Core Sample Research, JAMSTEC 5: Dept. of Earth & Planetary Sciences, McGill University 6. Dept of Earth, Planetary & Space Sciences, University of California, Los Angeles 7. Dept. of Geological Sciences, University of Colorado, Boulder 8. Tectonics & Geodynamics, RWTH Aachen University 9. Dept. of Earth, Environmental and Planetary Sciences, Brown University 10. Dept. of Earth Science, University of California, Santa Barbara 11. Dept. of Geological Sciences, University of Texas, Austin 12. Dept. of Earth Science, University of Bergen … 13. Dept. of Ocean & Earth Science, National Oceanography Centre Southampton 14. Alara Resources Ltd., Oman 15. School of Geography, Earth and Environmental Sciences, University of Plymouth …16. Dept. of Earth & Planetary Sciences, Nagoya University 17. Dept. of Geology, Niigata University & VERC IMG JAMSTEC 18. Oman Water Society & Middle East Desalination Research Center

Abstract

This paper provides an overview of research on core from Oman Drilling Project Hole BT1B and the surrounding area, plus new data and calculations, constraining processes in the Tethyan subduction zone beneath the Samail ophiolite. The area is underlain by gently dipping, broadly folded layers of allochthonous Hawasina pelagic sediments, the metamorphic sole of the Samail ophiolite, and Banded Unit peridotites at the base of the Samail mantle section. Despite reactivation of some faults during uplift of the Jebel Akdar and Saih Hatat domes, the area preserves the tectonic "stratigraphy" of the Cretaceous subduction zone. Gently dipping listvenite bands, parallel to peridotite banding and to contacts between the peridotite and the metamorphic sole, replace peridotite at and near the basal thrust. Listvenites formed at less than 200°C and (poorly constrained) depths of 25 to 40 km by reaction with CO_2-rich, aqueous fluids migrating from greater depths, derived from devolatilization of subducting sediments analogous to clastic sediments in the Hawasina Formation, at 400-500°. Such processes could form important reservoirs for subducted CO_2. Listvenite formation was accompanied by ductile deformation of serpentinites and listvenites – perhaps facilitated by fluid-rock reaction – in a process that could lead to aseismic subduction in some regions. Addition of H_2O and CO_2 to the mantle wedge, forming serpentinites and listvenites, caused large increases in the solid mass and volume of the rocks. This may have been accommodated by fractures formed as a result of volume changes, mainly at a serpentinization front.

Plain language summary

This paper reports initial results from study of core from Oman Drilling Project Hole BT1B and the surrounding area. It provides insights into subduction zone processes, including large fluxes of recycled CO_2 from subducting sediments into the leading edge of the mantle wedge, and surprisingly low temperature ductile deformation at less than 200°C. Recycling of CO_2 via carbon mineralization in the hanging wall of subduction zones may produce an important, lithospheric reservoir in the global carbon cycle. Ductile deformation of serpentinite, and during or after transformation of peridotite to listvenites (mixtures of carbonates and opal or quartz) could explain aseismic subduction atop some subduction zones.

1. Introduction

Oman Drilling Project (OmanDP) Hole BT1B at 23.364374°N, 58.182693°E, about 12 km southeast of the town of Fanjah in the Sultanate of Oman, sampled serpentinized peridotites and listvenites (fully carbonated peridotites, Halls & Zhao 1995) at the base of the Samail ophiolite, the basal fault of the ophiolite, and the underlying metamorphic sole, with the intention of investigating mass transfer and deformation in the "leading edge of the mantle wedge" overlying a Tethyan subduction zone. Study of outcrops along the contact between the sole and the peridotite can illuminate processes in and above a subduction zone that are generally inaccessible to direct observation. Of particular interest are (a) the source of footwall fluids, (b) the nature and mechanism of fluid transport along the thrust fault and into the mantle wedge, (c) chemical, mineralogical and rheological modification of the hanging wall by reaction with footwall fluids, and (d) the mechanisms of subduction zone deformation.

Hole BT1B was drilled using cylindrical diamond bits and wireline core retrieval, from March 7 to March 23, 2017. Core recovery was ~ 100% throughout the Hole. Core was shipped to Japan and loaded onto Drilling Vessel Chikyu, where the OmanDP Science Team performed analyses closely following protocols established by the various incarnations of the Ocean Drilling Program (currently, the International Ocean Discovery Program, IODP). Detailed core descriptions, together with drilling history and some background information (Kelemen et al 2020b, Kelemen et al 2020c) are available online at http://publications.iodp.org/other/Oman/VOLUME/CHAPTERS/113_BT1.PDF

This paper reports new mapping and structural observations, mineral analyses and modeling, together with a summary of prior observations. It is intended to provide interpretive context for more detailed studies of core from Hole BT1B and the geology of the surrounding region. Such studies in this Special Issue of the Journal of Geophysical Research include those focused on textural and petrologic data for listvenites (Beinlich et al 2020) and the metamorphic sole (Kotowski et al 2021), volume changes during serpentinization (Malvoisin et al 2020), major and trace element geochemistry with relevance to subduction zone mass transfer (Godard et al 2021, Okazaki et al 2021), Mg-, Sr- and C-isotope geochemistry constraining the source of CO_2-bearing fluids and the fluid-rock reaction process (de Obeso et al 2021a, de Obeso et al 2021b) and deformation of the listvenites (Menzel et al 2020, Menzel et al 2021).

Section 2 provides geological context for observations of core and surrounding outcrops. Section 3 summarizes methods used to produce results presented for the first time in this paper. Section 4 reports new geological field observations and analytical data, and reviews key results from Kelemen et al. (2020b) in context. Section 5 discusses the pressure, temperature and timing of listvenite formation, the nature and source of the fluids that transformed mantle peridotite into serpentinite and listvenite, the chemical and mechanical processes during these transformations, and deformation of altered mantle peridotite immediately above a paleo-subduction zone beneath the "leading edge of the mantle wedge".

It is hoped that this paper, and the other papers in this Special Issue, will provide a starting point for future investigations of this unique and important site. In this context, readers should be aware that the archive half of the core is currently stored at Petroleum Development Oman where it is available for viewing, the working half of the core is stored at the American Museum of Natural History, where it can be sampled upon request to the Museum, and a huge volume of data from shipboard visual core observations and analytical data is available to anyone at http://publications.iodp.org/other/Oman/OmanDP.html , https://www.icdp-online.org/projects/world/asia/oman/, and other sites that can be accessed from there.

2. Geological setting

2.1 Regional geologic context

The Samail ophiolite is composed of oceanic crust formed at a submarine spreading center above a subduction zone. The crustal thickness and composition of the ophiolite is similar to the geophysically and geologically constrained characteristics of fast-spreading, Pacific oceanic crust, with a few km of submarine lavas and sheeted dikes overlying a thicker, gabbroic lower crust (e.g., Christensen & Smewing 1981, Coleman & Hopson 1981, Nicolas et al 1996) However, the lavas have a trace element "subduction signature" (Alabaster et al 1982, Pearce et al 1981, Pearce & Peate 1995), and parental, mantle-derived magmas appear to have contained 0.2 to 2 wt% H_2O, substantially more than in primitive mid-ocean ridge basalts (MacLeod et al 2013). Beneath the crustal section of the ophiolite, residual mantle peridotites and tabular dunites record polybaric decompression melting, melt extraction, and focused transport of basaltic melt upward to form the crust (Braun & Kelemen 2002, Godard et al 2000, Kelemen et al 2000, Kelemen et al 1995, Monnier et al 2006).

2.2 Lithologies at the base of the Samail ophiolite

Here we describe the units above and below the basal fault of the Samail ophiolite. We begin with a review of work on the metamorphic sole. Then, we describe the overlying Banded Unit at the base of the ophiolite's mantle section. Finally, we briefly outline the nature of the sedimentary rocks beneath the metamorphic sole.

Beneath the mantle section of the ophiolite, and above allocthonous sediments of the Hawasina Formation, are discontinuously exposed lenses of a "metamorphic sole". Peak pressures and temperatures in the sole generally record hot subduction conditions at temperatures up to 700-900°C (Cowan et al 2014, Ghent & Stout 1981, Hacker & Gnos 1997, Searle & Cox 1999, Searle & Cox 2002, Searle et al 1980, Searle & Malpas 1980, Searle & Malpas 1982, Soret et al 2017) though at BT1B peak temperatures are 450-550°C (Kotowski et al 2021). Apparently – based on published data and calculations – the sole records a broad range of peak pressures from a possible lower limit of 200

MPa (Ghent & Stout 1981) or 800 MPa (Soret et al 2017) to a possible upper limit of 1400 MPa (Cowan et al 2014, Searle & Cox 2002). Kotowski et al. (2021) report that the sole in core from Hole BT1B records a peak pressure in the range of 800 to 1200 MPa.

The sole contains metasediments and meta-volcanic rocks – including submarine pillow lavas – with the major element compositions of mid-ocean ridge basalts (MORB) as well as alkali basalts and more evolved andesites and dacites (Alabaster et al 1982, Ernewein et al 1988, MacLeod et al 2013, Pearce et al 1981, Searle et al 1980). In core from BT1B, alkaline metabasalt compositions in the sole (Godard et al 2021, Kelemen et al 2020c) are unlike the magmas that formed the crust of the Samail ophiolite. In the ophiolite, the structurally lowest, “Geotimes” or “V1” lavas are similar to normal mid-ocean ridge basalts, though they probably were hydrous and they contain a hint of an arc trace element signature (Alabaster et al 1982, Ernewein et al 1988, MacLeod et al 2013, Pearce et al 1981). Their composition, and that of dunite conduits for transport of primitive melts parental to V1 through the shallow mantle, is consistent with formation of the gabbroic lower crust in the Samail and Wadi Tayin massifs of the ophiolite from primitive V1 magmas (Braun & Kelemen 2002, Kelemen et al 1997, Kelemen et al 1995). The overlying “Lasail” or “V2” lavas in the ophiolite are incompatible-element-depleted, with a stronger subduction signature (Alabaster et al 1982, Ernewein et al 1988, MacLeod et al 2013, Pearce et al 1981) and include boninites (e.g., Ishikawa et al 2002) as well as tholeiitic basalts, andesites and dacites. Neither V1 nor V2 lavas are similar to the alkali basalt compositions in the sole. The present day $^{87}Sr/^{86}Sr$ ratios in the alkali basalts in core from BT1B range from 0.704 to 0.706 (de Obeso et al 2021a), more radiogenic than MORB. Though their Sr isotope ratio may have been modified by alteration, one possibility is that the alkali basalts are remnants of subducted seamounts with elevated $^{87}Sr/^{86}Sr$, similar to accreted seamounts along the Cascadia margin of North America (e.g., Duncan 1982).

In addition to metabasalts, regionally the sole contains metasediments, and “exotic limestones”, all incorporated by Searle and Malpas (1980) in the “Haybi Formation”. However, in this paper we informally group the Haybi Formation into an undifferentiated metamorphic sole unit. In the sole sampled by drill core from Hole BT1B, metasediments are clearly distinguishable from the metabasalts based on texture, but some of them are compositionally similar to the metabasalts, perhaps reflecting a volcanoclastic origin, whereas others grade into somewhat odd, low-SiO_2, muscovite-bearing lithologies (Godard et al 2021, Kelemen et al 2020b, Kotowski et al 2021).

Above the sole – where it is present – and elsewhere at the base of the ophiolite, the lower few km of the mantle section contains easily visible, meter to 10-meter scale, parallel bands of dunite, harzburgite and (rare) lherzolite, informally known as the Banded Unit (Godard et al 2000, Khedr et al 2013, Khedr et al 2014, Linckens et al 2011, Lippard et al 1986, Prigent et al 2018a, Prigent et al 2018b, Takazawa et al 2003, Yoshikawa et al 2015). The lithological contacts in this unit are sharp. They have low angle dips with respect to the paleo-seafloor, the crust-mantle transition zone, and the basal fault that juxtaposes mantle peridotite with the metamorphic sole. Mylonitic shear zones are

present in the Banded Unit , with textures recording deformation at 700–1,000°C (Boudier et al 1988, Herwegh et al 2016, Linckens et al 2011, Prigent et al 2018a). Thus, there is evidence for high strain ductile deformation and transposition of layering at the base of the mantle section, which might have accommodated substantial thinning (Prigent et al 2018a, Soret et al 2017). Similarly, there is evidence for thinning of the units below the ophiolite (Grobe et al 2018, Grobe et al 2019).

While some of the range in temperature and pressure estimates from the sole and the Banded Unit may be due to analytical and methodological uncertainty, or incomplete preservation and sampling of the highest-grade rocks, some may be due to temporal and spatial variability in peak metamorphic conditions. Moreover, the temperature record may be biased toward peak conditions, rather than later cooling. At the initiation of subduction near a spreading ridge, hot metamorphic rocks from the footwall may be accreted to the hot base of the newly formed mantle wedge, whereas as subduction zones grow colder and develop a steady-state thermal structure, cold dense lithologies in the footwall may be subducted (Agard et al 2016, Soret et al 2017). If so, the metamorphic sole in Oman may record the anomalously high temperatures of subduction initiation, and not the lower temperatures of evolution toward a steady-state subduction zone geotherm. The relatively low temperatures recorded by the sole in BT1B core could represent a point along this cooling path (Kotowski et al 2021).

A close correspondence between 96 to 95 Ma igneous ages in the crust, and both $^{40}Ar/^{39}Ar$ and zircon U/Pb ages of metamorphic rocks along the basal thrust (ca. 96-94 Ma), indicates that thrusting of the Samail ophiolite over adjacent oceanic crust and nearby pelagic sedimentary units began during formation of igneous crust in the ophiolite (e.g. , Garber et al 2020, Hacker & Gnos 1997, Hacker & Mosenfelder 1996, Hacker et al 1996, Rioux et al 2012, Rioux et al 2013, Rioux et al 2016, Rioux et al 2021b, Stanger 1985, Styles et al 2006, Tilton et al 1981, Warren et al 2005) or perhaps even earlier (Guilmette et al 2018).

The base of the metamorphic sole is truncated by a fault contact with autochthonous, low-grade metasediments of the Hawasina Formation, composed of pelagic clastic units interlayered with limestones (Béchennec et al 1990, Béchennec et al 1988). Relatively high, age corrected $^{87}Sr/^{86}Sr$ ratios in the clastic units suggest that they are distal sediments derived from erosion of continental crust (de Obeso et al 2021a, Weyhenmeyer 2000), while carbonate units record Sr isotope ratios similar to those of Mesozoic seawater (Weyhenmeyer 2000, Wohlwend et al 2017). These sedimentary units were thrust over Mesozoic to Proterozoic rocks of the Arabian continental margin, forming a “rumpled rug” between the autochthon and the ophiolite throughout northern Oman and the eastern United Arab Emirates.

2.4 History of the basal thrust of the Samail ophiolite

Where the metamorphic sole is preserved, its tectonic contact with the mantle section of the ophiolite represents a paleo-subduction zone at the base of the ophiolite, which consumed several hundred

kilometers of Tethyan basin and then continental crust before coming to rest on the Arabian continental margin (Béchennec et al 1990, Béchennec et al 1988, Breton et al 2004, Cooper 1988, Ninkabou et al 2021, Searle & Robertson 1990, van Hinsbergen et al 2019). During this time, the overlying peridotite was “the leading edge of the mantle wedge”.

During coeval metamorphism of the sole and igneous accretion of the crust in the ophiolite, the relative locations of these two units are uncertain. Primitive V1 magmas in the ophiolite, with compositions almost indistinguishable from mid-ocean ridge basalts (MORB), crystallized to form most of the crust, particularly in the southern Wadi Tayin and Samail massifs that were the site of of the OmanDP boreholes. Like MORB worldwide, these magmas probably formed via polybaric decompression melting over a depth interval of 75 km or more (e.g., Allegre et al 1973, Asimow et al 2004, Bottinga & Allegre 1973, Klein & Langmuir 1987, McKenzie & Bickle 1988). Thus, the metamorphic sole (recording peak depths less than 40 km) must not have been directly beneath the spreading center during crustal formation and metamorphism. Instead, the ophiolite section and the metamorphic sole were juxtaposed after crust formation and after peak metamorphism in the sole.

Moreover, the structural thickness of the Samail ophiolite measured perpendicular to the paleo-seafloor and/or the crust/mantle transition zone, and including both crust and mantle sections, never exceeds ~ 20 to 30 km (Boudier & Coleman 1981, Nicolas et al 2000), corresponding to a pressure less than or equal to ~ 800 MPa, beneath ~ 7 km of crust (on average, Nicolas et al 1996) and up to ~ 20 km of fresh mantle peridotite. Thus, the structural thickness of the ophiolite appears to be at least 10 km less than the depth inferred from the high end of the pressure range recorded by the sole (1300 or 1400 MPa, ~ 40 to 45 km). In addition, there is no evidence for widespread, tectonic thinning of the crustal section of the ophiolite, either by faulting or ductile deformation.

How can these data be reconciled? One possibility is that the peak pressures inferred for the sole are imprecise, and/or that they represent tectonic “overpressures” that don’t correspond closely with depth (Garber et al 2020). In this interpretation, the metamorphism of the sole could have occurred at ~ 800 MPa, corresponding to the current structural thickness of the ophiolite. A second possibility, as noted above, is that the base of the mantle section of the ophiolite underwent tectonic thinning, perhaps via simple shear (Prigent et al 2018a, Soret et al 2017). A third alternative is that some of the lenses of the metamorphic sole – those recording the highest pressures - migrated updip to reach their current structural position, ~ 25 km below the paleo seafloor. Indeed, upward transport of buoyant footwall lithologies during subduction is recorded in many preserved collisional orogens (e.g., Chemenda et al 2000). If so, updip migration of the sole with respect to the overlying ophiolite must have occurred after peak metamorphism but during Tethyan subduction, prior to emplacement of the ophiolite and the sole over the allochthonous Hawasina sediments. Finally, of course, it is possible that the current juxtaposition of the sole and the base of the ophiolite may be explained as the result of combinations of these three alternatives.

Subsequent events have affected the wedge, the sole, the underlying sedimentary units, and the faults between them (Grobe et al 2018, Grobe et al 2019). The end of subduction and emplacement of the ophiolite over allochthonous Hawasina sediments and the autochthonous, Arabian continental margin was followed by subaerial erosion, and then by a marine transgression marked by deposition of shallow water limestones at ~ 74 Ma (Al Khirbash 2015, Alsharan & Nasir 1996, Bailey 1981, Hansman et al 2017a, Nolan et al 1990, Schlüter et al 2008, Wyns et al 1992). Then, large scale uplift deformed all these units, forming the gigantic Jebel Akdar and Saih Hatat domes, cored by Proterozoic continental crust (e.g., Glennie et al 1973, Glennie et al 1974b). Saih Hatat uplift and cooling started at about 60 Ma, if not earlier (e.g., Grobe et al 2018, Grobe et al 2019, Hansman et al 2017b). Doming reactivated and cut the basal thrust of the ophiolite in normal faults and shear zones. Some of these younger faults juxtaposed mantle peridotite from the ophiolite with the allochthonous Hawasina sedimentary rocks, and even with the autochthonous platform carbonates of the Arabian continental margin, along tectonic contacts where the metamorphic sole is no longer present.

However, despite these complexities, we reiterate that – where it is parallel to banding and foliation – the contact between the metamorphic sole and the overlying Banded Unit at the base of the Samail ophiolite mantle section represents the basal thrust of the ophiolite. In this paper, when we refer to the "basal thrust", we are referring to contacts that preserve these characteristics. In turn, though of course there can have been imbrication and/or subduction erosion, the basal thrust of the ophiolite represents the locus of 100's of kilometers of subduction of oceanic crust, overlying sediments and, ultimately, the Arabian continental margin.

2.5 Geology of MoD Mountain

Hole BT1B is on the north side of the wide Wadi Mansah, southeast of "Ministry of Defense Mountain", (MoD Mountain), which is informally named for the military firing range on the south side of Wadi Mansah. The MoD Mountain region is close to the saddle between the northeastward plunging end of the Jebel Akdar massif, to the west, and the westward plunging Saih Hatat massif to the northeast (Figure 1).

This region preserves a gently folded, tectonic "stratigraphy" (Figures 2 , 3 and 4). The lowest exposed units in this sequence, northeast of Hole BT1B, are diagenetically-altered sedimentary rocks, mostly clastic shales and slates with a few meter to 10 meter scale intercalations of limestone and minor lenses of metavolcanic rocks. These are parts of the Hawasina Formation (Béchennec et al 1990, Béchennec et al 1988). Overlying the Hawasina Formation is one of the most aerially extensive outcrops of the metamorphic sole in Oman and the UAE (e.g., Figure 1 and geologic maps in Soret et al 2017, Wilde et al 2002). The outcrop area is unusually large in this region because the unit is regionally flat lying, though broadly folded.

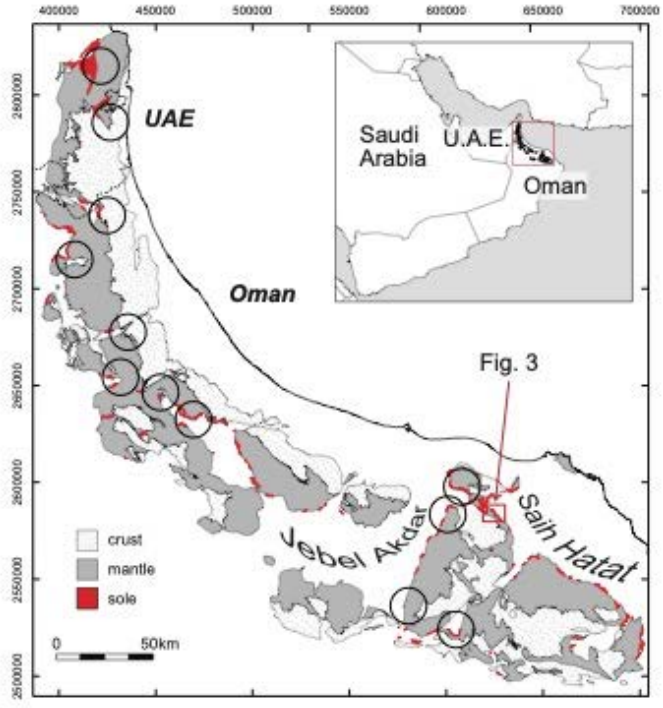

Figure 1: Outcrop area of the Samail ophiolite in Oman and the UAE, based on Nicolas et al. (2000). Metamorphic sole, in red. Black circles indicate approximate location of listvenites (Nasir et al 2007, Stanger 1985, Wilde et al 2002). Red rectangle indicates the approximate location of Figure 3, a geologic map of MoD Mtn and vicinity, which was the site of Oman DP Hole BT1B, and the focus of this paper.

Figure 2: Photograph of the west end of the MoD Mountain ridge, from the SW, looking NE, showing bands of listvenite (rusty orange) parallel to contacts between partially serpentinized harzburgite (brown) and dunite (tan) comprising the "Banded Unit" at the base of the Samail ophiolite mantle section. Greenish metabasalts and metasediments of the metamorphic sole underlying the ophiolite are exposed along indistinct ridge in lower left. The listvenite band at top right is more than 100 m thick and extends for 1.5 kilometers along the length of the summit ridge. The listvenite band in the center of the photo is 15-20 m thick. Photo taken with a telephoto lens from ~ 23.35°N, 58.17°E, along azimuth ~ 030°.

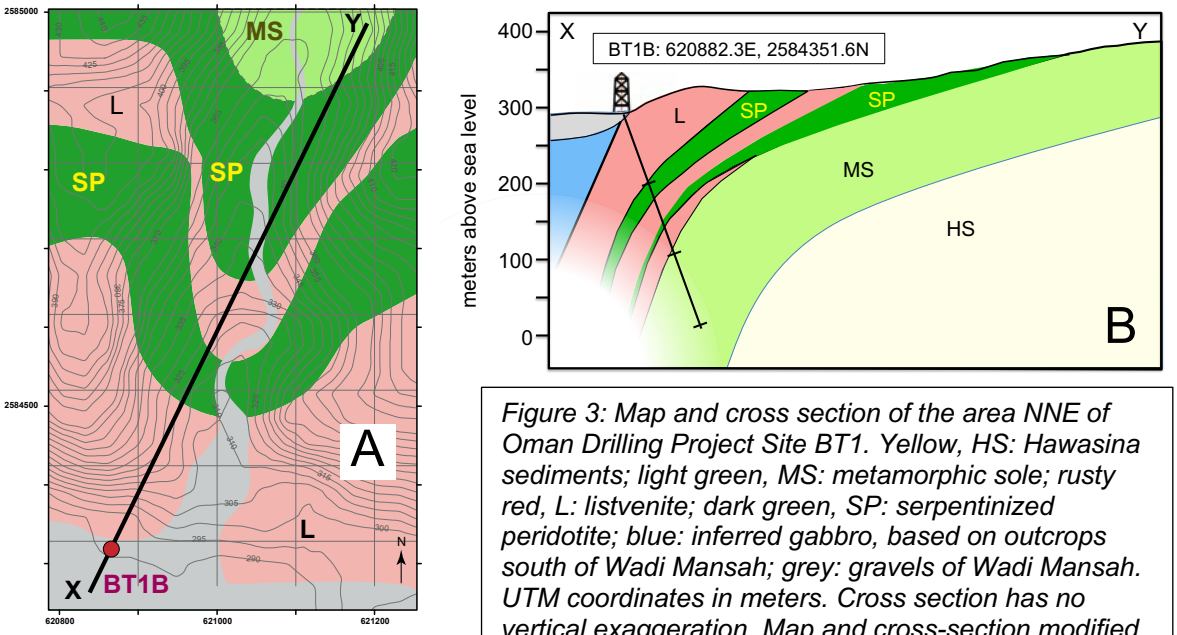

Figure 3: Map and cross section of the area NNE of Oman Drilling Project Site BT1. Yellow, HS: Hawasina sediments; light green, MS: metamorphic sole; rusty red, L: listvenite; dark green, SP: serpentinized peridotite; blue: inferred gabbro, based on outcrops south of Wadi Mansah; grey: gravels of Wadi Mansah. UTM coordinates in meters. Cross section has no vertical exaggeration. Map and cross-section modified from Figures F1 and F2 in Kelemen et al. (2020b)

Above the metamorphic sole in this gently folded "stratigraphy" is partially serpentinized peridotite, composed of distinctive, banded alternations of dunite, harzburgite and lherzolite on a scale of meters to tens of meters, characteristic of the "Banded Unit" at the base of the ophiolite (Boudier et al 1988, Boudier & Coleman 1981, Lippard et al 1986, Searle & Cox 2002). Indeed, partially serpentinized mantle peridotites on MoD Mountain, northeast of Hole BT1B have compositions similar to the Banded Unit elsewhere, and distinct from shallower, residual mantle peridotites of the Samail ophiolite emantle section, as discussed in Section 5.5, below. The presence of the Banded Unit overlying the metamorphic sole is another indication that MoD Mountain area exposes the basal thrust of the ophiolite – the paleo-subduction zone – together with the overlying mantle wedge.

In some localities, peridotites at the base of the Samail ophiolite mantle section have undergone 100% carbonation at ~ 100-200°C to form "listvenites" (Beinlich et al 2020, Falk & Kelemen 2015, Glennie et al 1974a, Nasir et al 2007, Stanger 1985, Wilde et al 2002), in which all Mg and Ca are in carbonate minerals, and silica derived from olivine and pyroxene has formed quartz or chalcedony. In Oman, such listvenites are most abundant on and around MoD Mountain northeast of Hole BT1B, where they form part of the gently folded tectonic "stratigraphy" we are discussing here. Listvenites on the flanks of MoD Mountain form discontinuous tabular lenses with low angle dips, 10 to 200 meters thick, parallel to the basal thrust and to lithological banding in the peridotite. These lenses occur along the basal thrust – between peridotite and the sole – and enclosed within the peridotite, up to 300 meters above the sole. Contacts in outcrop between listvenite and the surrounding, partially serpentinized peridotite are marked by strongly foliated, 100% serpentinized zones, 1 to > 20 m thick.

The lithological banding in the peridotite and the listvenite lenses dip gently south on the south side of MoD Mountain, north on the north slopes of the mountain, and then south again along and NE of the

wadi bounding MoD Mountain to the north (Falk and Kelemen 2015 and this paper, Section 4.2). Despite later faulting, these structures define a broad anticline with an axis approximately coincident with the summit ridge of MoD Mountain, and a syncline with an axis roughly coincident with the wadi northeast of MoD Mountain. Listvenites form erosion resistant dip slopes and the tops of small buttes outlining the folded stratigraphy.

Listvenites elsewhere in Oman and the UAE are found along the basal thrust, commonly juxtaposed with, or within a few km of, the metamorphic sole and/or the Banded Unit at the base of the Samail mantle section, as at MoD Mountain. In some other outcrops, listvenites form lenses within broad serpentinite mélange zones at the base of the ophiolite (Nasir et al 2007, Stanger 1985). In contrast, listvenites are not found within the peridotite more than a few kilometers away from the basal thrust of the ophiolite.

A Rb/Sr isochron on listvenite mineral separates (97 Ma ± 29 Ma 2σ, Falk & Kelemen 2015) is similar to the better determined, 96 to 94 Ma U/Pb ages of zircon in the metamorphic sole and igneous crust in the ophiolite. Based on the listvenite mineral isochron, there is a 67% probability that the listvenites are older than 82.5 Ma (average – 1σ), and a 93% probability that they are older than 75 Ma (1.5σ), before the end of subduction. Thus, geological observations (summarized above and in Section 4.2) together with the isochron data indicate that the listvenites formed via transfer of CO_2 and other components from subducting material – probably sediments and/or altered lavas – into the leading edge of the mantle wedge during Tethyan subduction and ophiolite emplacement. New geological data supporting this are presented in 4.2. Sections 5.6 and 5.7 provide thermodynamic modeling that quantifies this hypothesis.

As noted in Section 2.4, Paleocene to Miocene uplift of the nearby Jebel Akdar and Saih Hatat massifs may have caused reactivation of some older faults, and definitely formed new, younger faults in the MoD area. For example, shallow-level gabbros and sheeted dikes are juxtaposed with mantle peridotite and the metamorphic sole on a steep fault parallel to Wadi Mansah, just south of Hole BT1B (Villey et al 1986, Wilde et al 2002). In another possible example, Scharf et al. (2020) report early U/Pb formation or cooling ages (60 ± 16 and 58 ± 6 Ma) of calcite veins that cut listvenite, cataclasite and fault contacts between listvenite and post-emplacement, Late Cretaceous conglomerates.

3. Methods

Here we describe methods used for new data presented for the first time in this paper. Supplementary Section S2 provides methods for data illustrated in this paper, but previously reported elsewhere.

3.1 Geological mapping

Geological field work to produce the map and cross-section in Figure 4 spanned short visits over about a decade. Contacts and structural measurements were located by GPS at the time of measurement. The topographic profile for the cross section was constructed using Google Earth.

3.2 Raman spectroscopy

Analyses of minerals in thin section and rock slabs were conducted at the Raman Microspectroscopy Laboratory, University of Colorado-Boulder with a Horiba Scientific LabRam HR Evolution Raman microscope. Measurements used a 100 mW 532 nm laser, focused through a 50x (0.75 NA) microscope objective onto a ~2 μm spot. The laser power was modulated with neutral density filters to about 15 mW at the sample surface. Multiple (2-10) accumulations were coadded in order to filter spikes and improve signal to noise, and the acquisition time and accumulation number were adjusted to yield appropriate data quality. Data processing was performed using LabSpec 6 software (Horiba Scientific), including correction for instrumental artifacts and polynomial baseline fitting/subtraction. Raman mapping was performed using a motorized stage with 2 μm step size, and map datasets were fit using classical least-squares fitting with endmember spectra isolated from regions within the map using LabSpec 6 after data processing.

3.3 Thermodynamic calculations and modeling

The speciation and chemical mass transfer code EQ3/6 (Wolery 1992) was used to predict the compositions of coexisting solid and aqueous phases that evolved during interaction between representative lithologies from the MoD Mountain area and CO_2-bearing fluids. Thermodynamic data for minerals were mostly from Berman (1988). Data for pyrite and pyrrhotite were from Helgeson et al. (1978). For aqueous species, thermodynamic data used in the simulations were calculated using the Deep Earth Water (DEW) model (Huang & Sverjensky 2019, Sverjensky et al 2014) which uses recent experimental and theoretical advances (Facq et al 2016, Pan et al 2013) to expand the extended Helgeson-Kirkham-Flowers (HKF) aqueous equation of state (Shock et al 1992, Shock et al 1997) to pressures up to 6.0 GPa.

The composition of 5 wt% aqueous fluid in equilibrium with a pelitic lithology from the Oman Hawasina Formation at 400 – 600°C and 0.5 to 2.0 GPa at low water/rock ratios was used. Specifically, a dilute fluid was equilibrated with the rock composition of sample OM20-17 (de Obeso et al 2021a), containing 0.06 wt% total carbon (Supplementary Table 2). The CaO content of OM20-17 was below detection. For the model calculations it was assumed to 0.1 wt%. In addition, the S content of this sample has not been measured. For this calculation it was assumed 100 ppm. At these high temperatures and low carbon contents, carbonate minerals are unstable and all carbon in the rock will be mobilized into the fluid phase as dissolved CO_2.

We calculated the outcome of cooling and decompression of the CO_2-rich fluid from OM20-17, to 100 – 300 °C and 0.5 to 2.0 GPa. This had no significant effect on its composition. We then calculated the products of reaction between this fluid and average Oman harzburgite (Supplementary Table 2, calculated from Godard et al 2000, Hanghoj et al 2010, Monnier et al 2006) at 100 – 300 °C and 0.5 – 1.0 GPa, at water:rock ratios ranging from 100 to 1.

As a result of data limitations, solid solutions of precipitating minerals were not considered, as the Berman database lacks properties for most Fe-endmembers of minerals commonly observed in listvenites and associated rocks. Thus, for example, the model predicts co-precipitation of pure, endmember magnesite, dolomite and siderite, whereas in listvenite samples we observe Fe-bearing magnesite and dolomite. Among the serpentine polytypes, only chrysotile precipitation can be modeled. We did not include goethite. There are no thermodynamic data for a chromian muscovite component, so this was not included, despite the fact that solid solutions ranging from fuchsite to chromian muscovite are observed in MoD Mountain listvenites (e.g., Falk & Kelemen 2015).

Phase equilibrium calculations constraining the conditions for co-existing graphite (± amorphous carbon compounds) and hematite, and updated calculations for co-existing antigorite and quartz, used (1) Thermocalc (Powell et al 1998), (2) Perple_X (https://www.perplex.ethz.ch/) (Connolly 1990, Connolly 2005, Connolly 2009), with the Holland and Powell thermodynamic data for minerals (2003, 1998), and the default equations of state for H_2O- CO_2 fluids (modified versions of Redlich-Kwong), and (3) SUPCRT (Johnson et al 1992, Zimmer et al 2016) with thermodynamic data for minerals from Helgeson et al. (Helgeson 1985, 1978) or Berman (1988, plus graphite from Helgeson et al.) and various equations of state for H_2O-CO_2 fluids (Shock et al 1992, Shock et al 1997) modified from Helgeson et al. (1981). All of these different combinations provided consistent results, with antigorite + quartz stable with respect to talc at temperatures up to 80 to 120*C. However, calculations using the Deep Earth Water (DEW) model (Huang & Sverjensky 2019, Sverjensky et al 2014) and the extended Helgeson-Kirkham-Flowers (HKF) aqueous equation of state (Shock et al 1992, Shock et al 1997) do not predict equilibrium coexistence of antigorite + quartz above 15°C.

3.4 (U,Th)/He ratio measurements and cooling age calculation

All (U-Th)/He analyses were completed at the UTChron facility at the University of Texas at Austin, using aliquots of zircon separates from the metamorphic sole and lower crustal gabbros, previously analyzed for U/Pb ages by Rioux et al. (in prep.), following procedures of Wolf and Stockli (2010). Individual zircon grains were morphometrically characterized to determine alpha ejection correction (Ft, Farley et al., 1996; Cooperdock et al., 2020), equivalent spherical radius (ESR), and estimated mass assuming a tetragonal prism. Single-grain zircon sample aliquots were loaded into Pt tubes for in-vacuo laser He heating for 10 min at ~1200°C by diode laser and 4He concentrations were measured by isotope dilution, using a ^{3}He tracer, on a Blazers Prisma QMS-200 quadrupole mass spectrometer, after cryogenic purification. Blanks and ^{4}He gas standards were run between unknowns

to monitor and quantify the procedural baseline during analytical runs. Aliquot laser reheating was repeated (2-5x) until 4He gas yields dropped <1% total extracted gas.

After degassing, individual zircon grains were removed from the Pt packets and dissolved using a two-step HF-HNO_3 and HCl pressure vessel dissolution technique and measured on a Thermo Element2 HR-ICP-MS following the procedure outlined in Wolf and Stockli (2010). U-Th-Sm concentrations were calculated using isotope dilution with an isotopically enriched, mixed U-Th-Sm spike calibrated against a 1 ppb U-Th-Sm gravimetric standard solution and blank-corrected using the average of multiple procedural blanks.

Final (U-Th)/He ages were calculated using blank corrected U, Th, Sm and He measurements for each aliquot. Reported concentrations were determined using the morphometrically determined mass of each aliquot. The reported error for individual (U-Th)/He ages represents standard error (8%) based on long-term intra-laboratory reproducibility of Fish Canyon tuff zircon standard, following the approach of Farley et al. (2001). The reported mean sample ages reflect the arithmetic mean of the aliquot ages and their standard deviations.

3.5 Calibration of XRF core scanner data

XRF core scanner data were collected onboard DV Chikyu, as described in Kelemen et al. (2020b). We used the core scanner to analyze nine listvenite samples from BT1B core, and 14 gabbro samples from Hole GT1A core that had known bulk compositions based on XRF analysis at the University of St. Andrews. While onboard DV Chikyu, we used the St. Andrews data to calibrate the XRF data, as follows: wt% SiO_2 = 0.89 x (scanner wt% SiO_2); wt% MgO = 2.57 + 1.18 x (scanner wt% MgO); wt% FeO^T = 1.048 + (scanner wt% FeO^T)^0.848; and wt% CaO = 0.878 x (scanner wt% CaO), where FeO^T indicates all Fe is treated as FeO. Fits are illustrated in Supplementary Figure 2. Okazaki et al. (2021) present a comprehensive analysis of the XRF scanner data, together with X-Ray tomography data for BT1B core.

3.6 Calculation of mineral volume proportions

Volume proportions of quartz, magnesite and dolomite were estimated from bulk rock compositions and XRF scanner data as follows. Weight fractions of SiO_2, MgO, FeO^T and CaO were converted to moles in 100 grams of rock using their molecular weights. (For all data reported in this paper, the sum of wt% SiO_2, MgO, FeO^T and CaO was greater than 90% of the volatile free, bulk rock composition). The number of moles of dolomite were taken to be equal to moles of CaO, moles of magnesite were calculated as moles MgO – moles CaO, and moles of quartz were taken to be equal to moles of SiO_2. All Fe was inferred to be in Fe-oxides and hydroxides. If the small amounts of Fe in carbonate minerals were included in such a calculation, this would slightly increase the proportions of magnesite and dolomite, relative to quartz. Volumes of each mineral in 100 grams of rock were calculated using

their molar volumes. The data were “projected” from Fe oxy-hydroxides by normalizing the volumes of quartz, magnesite and dolomite to 100%.

4. Results

4.1 Drilling operations

Site BT1 is on the north side of the broad channel of Wadi Mansah, which drains mountainous regions to the east and southeast. Hole BT1A penetrated 1.90 meters of gravels in Wadi Mansah, south of listvenite outcrops flanking the Wadi. After we became concerned that a steep hole there might intersect tens of meters of gravel before reaching bedrock, and/or that the gravel might overlie a major, steep fault along Wadi Mansah that postdates ophiolite emplacement, we moved the drill and inclined the Hole. Hole BT1B is three or four meters closer to the listvenite outcrop. The well head is intact, marked and protected from floods by a concrete monument. Drilling of the fine-grained, silica-rich listvenites was challenging, because this lithology has a hardness similar to fine-grained chert or flint (~ 7 on the Mohs’ scale), but with patience and expert drilling, we obtained ~ 100% recovery of all lithologies intersected by the borehole. Details of drilling operations are in Kelemen et al. (2020b).

4.2 Mapping and structural observations

Geological mapping of the area around MoD Mountain, together with measurement of the orientation of lithological contacts, began in 2009, and continued via brief visits through 2019. As noted in Section 2.5, and reported by Falk and Kelemen (2015), the mountain is underlain by a southeast to northwest striking anticline, with its faulted hinge approximately coincident with the ridge along the summit. Exposed contacts between listvenite and serpentinized harzburgite consistently dip to the southwest on the southwest side of the mountain, and to the east and northeast on the northeast side. In the valley north of the mountain, listvenite-harzburgite, listvenite-metamorphic sole, and harzburgite-sole contacts form a broad, shallow syncline. A new, detailed geological map and cross-section, incorporating our lithological and structural observations, is presented in Figure 4.

As shown on the map, in outcrops extending for more than 4 km north of Hole BT1B there is a regular tectonic “stratigraphy”, with variably altered peridotite overlying the metamorphic sole, in turn overlying Hawasina Formation sediments, all with low angle fault contacts that have been deformed by a series of gentle, broad open folds evident in the map and cross-section.

We noted normal and reverse shear sense indicators on both sides of the anticline. As a result of the folding, it is difficult to interpret the sense of shear recorded in various outcrops. Some shear sense indicators may predate the folding, while others may record deformation during or after folding.

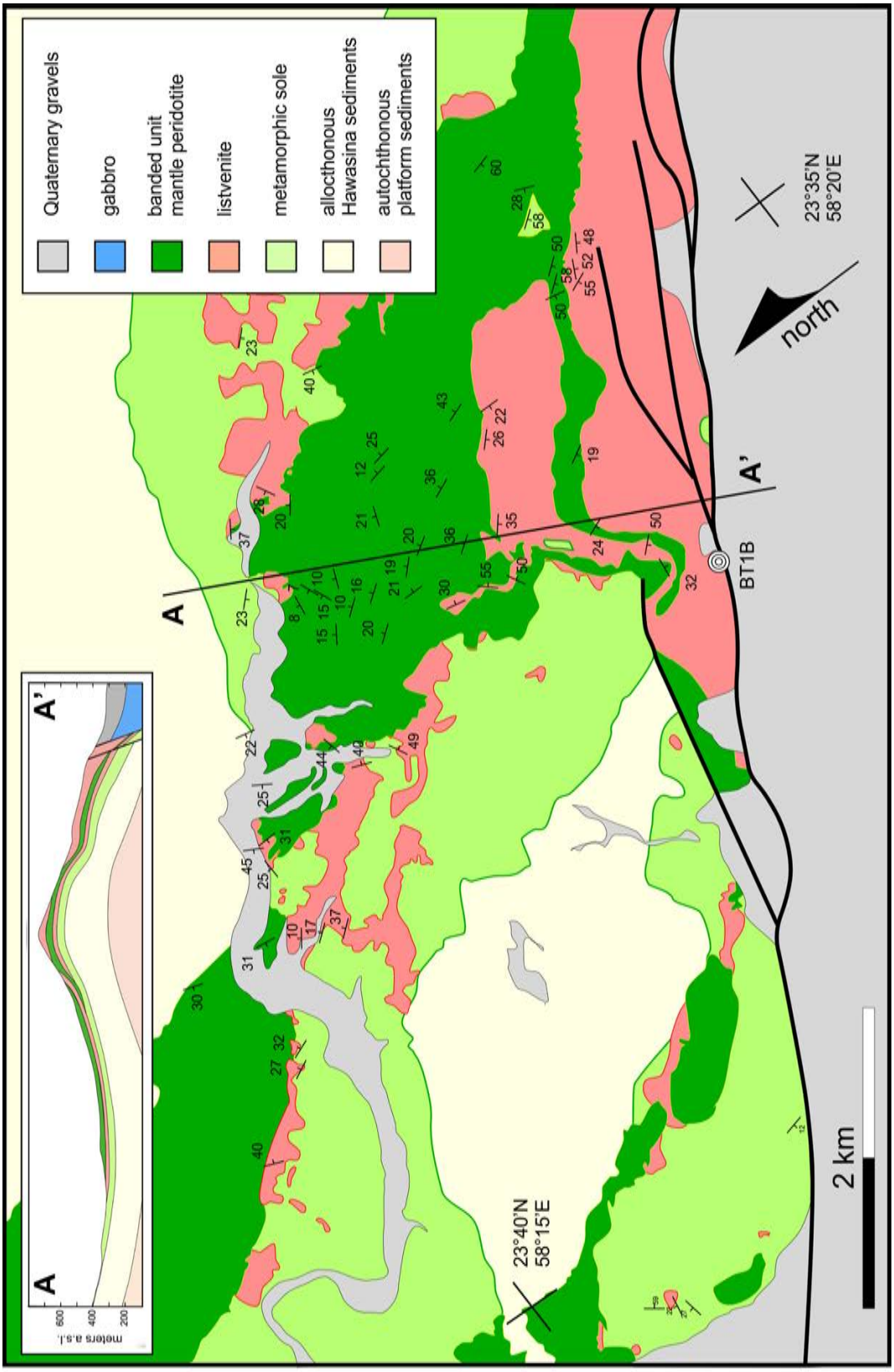

Figure 4: Geologic map and cross section of MoD Mountain and vicinity. Complex map pattern arises from intersection of topography with broadly folded, gently dipping units, as is more evident in the cross section (no vertical exaggeration) illustrating the antiform coinciding with MoD Mountain, and the syncline to its north. Dips are all measured on lithologic contacts, including dunite/harzburgite contacts within the Samail ophiolite mantle section.

In contrast, to the northwest and southeast, outside our map area, the outcrop patterns become much more complex, the sole outcrop thins, and there are some vertical fault contacts where all of these older units are juxtaposed with Late Cretaceous Al Khod conglomerates and younger, shallow marine limestones (Stanger 1985, Villey et al 1986, Wilde et al 2002).

4.3 Zircon (U,Th)/He cooling ages

Zircon (U,Th)/He cooling ages on samples from the metamorphic sole southeast of Fanjah, near MoD Mountain, are 38.7 ± 7.7 and 44.4 ± 8.0 Ma, cooling ages of zircons from the metamorphic sole at the base of the Wadi Tayin massif to the east are 54.5 ± 7.4 and 61.8 ± 2.6 Ma, and the cooling age of zircons from the lower crust of the Samail massif is 46.4 ± 3.9 Ma (Supplementary Table 1 and Supplementary Figure 1).

4.4 Lithology

As illustrated in Figure 5, the top of the Hole sampled ~ 200 meters of listvenite interlayered with two serpentinite bands from 80 to 100 m depth, and 181 to 185 m depth. Below 185 m, the listvenite is ubiquitously deformed, with visual core descriptions indicating a mixture of brittle and ductile deformation. At about 197 m, core was composed of a few tens of cm of soft, clay-rich fault gouge, together with a few cm of hard, aphanitic, black ultracataclasite. Beneath these fault lithologies, the core sampled ~ 102 meters of the metamorphic sole, grading from dominantly fine-grained, finely-banded, muscovite-bearing metasediments at the top (“greenschists” in Figure 5) to coarser, more massive-appearing, foliated “greenstones”, interpreted as metavolcanic rocks, at the bottom.

Serpentinite bands in the core have gradational contacts with host listvenites over 10’s of centimeters to ~ 1 m thick. Serpentinites contain antitaxial veins of magnesite with a median line composed of hematite and other Fe-oxides. There are prismatic terminations of magnesite crystals away from vein centers, toward the host serpentine (Figure 6). Antitaxial veins record growth of minerals outward from the vein center. They are commonly interpreted to open due to the “pressure of crystallization” (Durney & Ramsay 1973, Urai et al 1991). However, this interpretation is less clear in the serpentinites and listvenites of Hole BT1B, where the Mg in the carbonate is derived from the host rocks. To some degree these veins may replace, rather than displace, the host.

Away from the veins, serpentinites also contain up to 10% magnesite ovoids 10 to 100 microns in diameter, unevenly dispersed within a massive serpentine matrix. These magnesite vein and ovoid textures are abundant in the listvenites as well. Thus, the Shipboard Scientific Party suggested that they are indicative of incipient replacement of serpentinite by listvenite, grading from < 10% carbonate (and no quartz) in veins and ovoids to 100% fine-grained carbonate + quartz across sharp reaction fronts (Kelemen et al 2020b). Another notable feature is that some of the serpentinites are optically

isotropic in thin section, probably indicative of low temperature formation of poorly ordered or amorphous material with serpentine stoichometry (e.g., Andreani et al 2004).

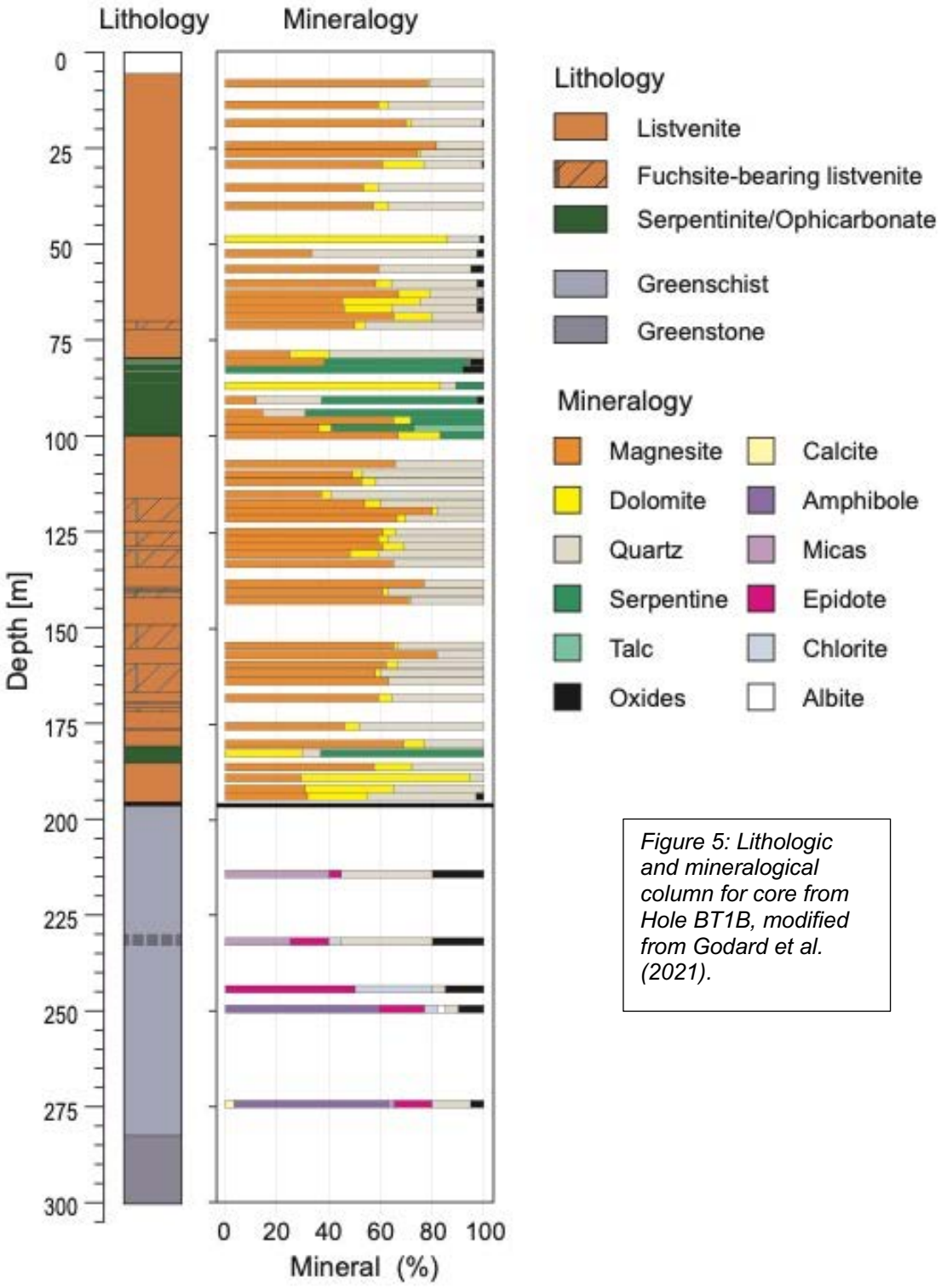

Figure 5: Lithologic and mineralogical column for core from Hole BT1B, modified from Godard et al. (2021).

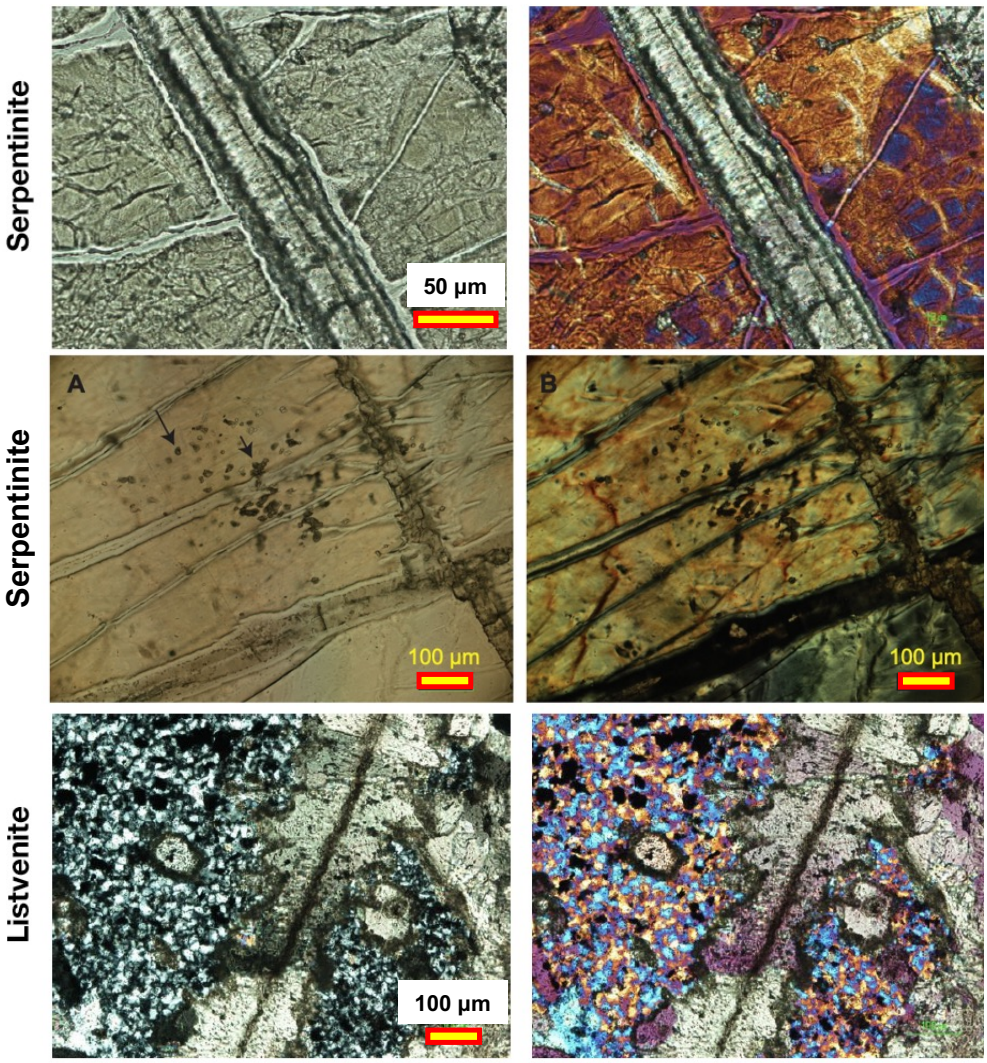

Figure 6: Antitaxial magnesite-hematite veins, and magnesite spheroids in serpentinites and listvenites in core from Hole BT1B. Top panels: plane light (left) and crossed-polarized images (right, quartz plate (+1λ) inserted) of magnesite-hematite veins near the lower contact of the upper serpentinite band, TS_BT1B_44Z-3_9-11.5, ~100 m depth, from Figure F47 in Kelemen et al. (2020b). Middle panels: tiny magnesite spheroids in serpentinite, TS_BT1B_44Z-3_9-11.5, ~100 m depth, from Figure F29 in Kelemen et al. (2020b). F. Bottom panels: Cross-polarized images, right one with quartz plate (+1λ) inserted, of texturally similar, "antitaxial" magnesite-hematite veins and magnesite ovoids in quartz-rich, listvenite matrix, TS_BT1B_47Z-3_15-19 at about 110 m depth, from Figure F35 in Kelemen et al. (2020b).

In turn, listvenites and serpentinites recovered in drill core are hosted by more typical, partially serpentinized peridotites and dunites in outcrop north and northeast of Hole BT1B (Figure 7). Such lithologies, typical of the Banded Unit at the base of the mantle section of the Samail ophiolite, are abundant on the flanks of MoD Mountain, and are particularly well exposed west of the summit (Figure 2) and on the broad, north facing outcrop below the summit ridge.

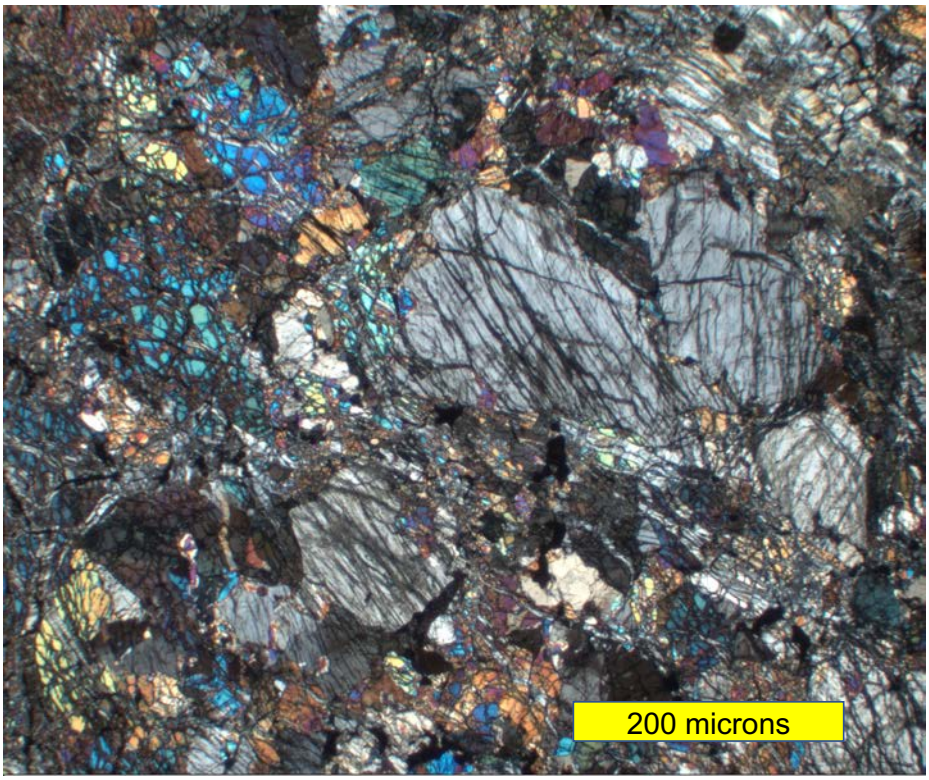

Figure 7: Cross-polarized image of partially-serpentinized harzburgite sample OM09-14 (Falk & Kelemen 2015) from ~ 10 m above lower listvenite band in Figure 2. Olivine: bright interference colors and irregular, serpentine-filled fractures. Orthopyroxene: grey interference colors and parallel to orthogonal fractures. Minor calcic-pyroxene and/or hornblende are barely visible in this image.

A sample transect on the ridge forming the drainage divide between Wadi Mansah (site of Hole BT1B) and the parallel wadi north of MoD Mountain documented a 5-meter scale progression from listvenite to serpentinite (with intergrown quartz and antigorite) to partially serpentinized peridotite containing relict olivine and orthopyroxene (Figure 5 in Falk & Kelemen 2015). Along that watershed transect, the presence of antigorite – rather than the serpentine polytypes lizardite and chrysotile – was attributed to high SiO_2-activity produced by reaction of olivine and serpentine to produce carbonate and quartz, since antigorite is more SiO_2-rich than the other polytypes.

However, the serpentinites in core from Hole BT1B are distinct from the serpentinized zone flanking listvenite on the ridge transect, and from the surrounding, partially serpentinized Banded Horizon harzburgites. Although quartz veins cut the serpentinite in the core, antigorite was not observed. Moreover, despite the presence of some orthopyroxene pseudomorphs ("bastites") in serpentinites, and a concerted effort to find relict mantle minerals, no olivine or pyroxene were detected in drill core. Taken together, field and core observations suggest that the contact between serpentinites and partially serpentinized peridotites is gradational over a few meters at most, approximately as sharp as the contact between listvenites and serpentinites. More on this in Sections 5.7 and 5.8, below.

Essentially, two types of listvenite were recovered, magnesite + quartz + iron oxide lithologies, and volumetrically less abundant, dolomite + quartz + iron oxide rocks, previously termed magnesite-

lisvenites and dolomite-listvenites (Falk & Kelemen 2015). Much of the core contains 0.5 to 3% relict chromian spinel, partially or fully altered to Fe-oxides. Instead or in addition, some samples contain minor amounts of Cr-rich white mica (fuchsite-muscovite solid solutions, supplementary Figure 7 in Falk & Kelemen 2015), in mm to cm scale, ovoid, microscopic intergrowths with quartz. These intergrowths are macroscopically evident in outcrop and core as cm-scale green spots, though in fact Cr-rich mica composes only a few percent of such spots, apparently has undergone alteration to clays in some samples, and was significantly damaged or removed during thin section preparation. As a result, fuchsite crystals recovered from BT1B core are not large enough for $^{40}Ar/^{39}Ar$ analyses. Figure 5 of Nasir et al. (2007) is a photomicrograph of crystalline fuchsite from another listvenite in Oman.

Macroscopic listvenite textures are characterized by abundant veins (10 to 200 veins more than 1 mm thick per meter of core, typically ~ 1 per cm) in a fine-grained matrix. In massive listvenites, the fine-grained matrix surrounding veins commonly contains ovoids of magnesite or quartz (Figure 8). Though they have similar textures, ovoids of the two different minerals are rarely adjacent to each other. Both commonly have Fe-oxides in their cores and/or in spherical zones. Microprobe analyses show that magnesite ovoids have low Fe cores, commonly rimmed with relatively Fe-rich magnesite (Beinlich et al 2020). They have sizes and shapes similar to the quartz spherulites.

Carbonate ovoids and cross-cutting magnesite-hematite veins are also observed in serpentinite bands in the core (Figure 6). Thus, the Shipboard Science Party considered it likely that many such veins initially formed within serpentinite, followed by formation of ovoids within surrounding serpentine, and then by replacement of the entire serpentinite matrix by carbonate + quartz (Kelemen et al 2020b). If so, in contrast to conventional interpretations of veins as relatively young features, “cross-cutting” their matrices, in this case the fine-grained listvenite matrix may postdate the earliest veins found within the matrix. This hypothesis is discussed further in Section 5.9

The quartz ovoids have the texture of “spherulites”, with radiating microscopic crystals producing a false, “uniaxial interference pattern” in cross-polarized light. Spherulites form during devitrification of amorphous opal as well as rhyolite glass, so Falk & Kelemen (2015) and the Shipboard Science Party (Kelemen et al 2020b) interpreted these as replacing opal, which would have been among the earliest SiO_2 minerals to form in many of the listvenites. Importantly, opal is commonly found in other listvenites and serpentine-magnesite associations worldwide (Abu-Jaber & Kimberley 1992, Aftabi & Zarrinkoub 2013, Akbulut et al 2006, Arisi Rota et al 1971, Barnes et al 1973, Beinlich et al 2010, Borojević Šoštarić et al 2014, Boschi et al 2009, Ece et al 2005, Jurković et al 2012, Lacinska & Styles 2013, Lapham 1961, Oskierski et al 2013a, Oskierski et al 2013b, Posukhova et al 2013, Quesnel et al 2016, Searston 1998, Ulrich et al 2014, Zarrinkoub et al 2005).

Vein types cutting this fine-grained matrix generally record a progression from texturally early, antitaxial magnesite veins – some with cores of hematite + other Fe-oxides (Figure 6) – and related, early Fe-oxide veins, to syntaxial dolomite veins and carbonate-quartz veins, and lastly to syntaxial

calcite veins. Some of the late, syntaxial veins contain vugs lined with prismatic calcite and/or dolomite. Syntaxial vein textures record inward crystallization of crystals into fractures that opened due to external, tensional stresses (Durney & Ramsay 1973, Urai et al 1991).

(A poorly exposed, weathered, fuchsite vein has been observed in outcrop 200 meters north of Site BT1B, but no such veins were sampled in BT1B core. We mention this simply to emphasize that Cr and Al were mobile at some stage during listvenite formation or later alteration.)

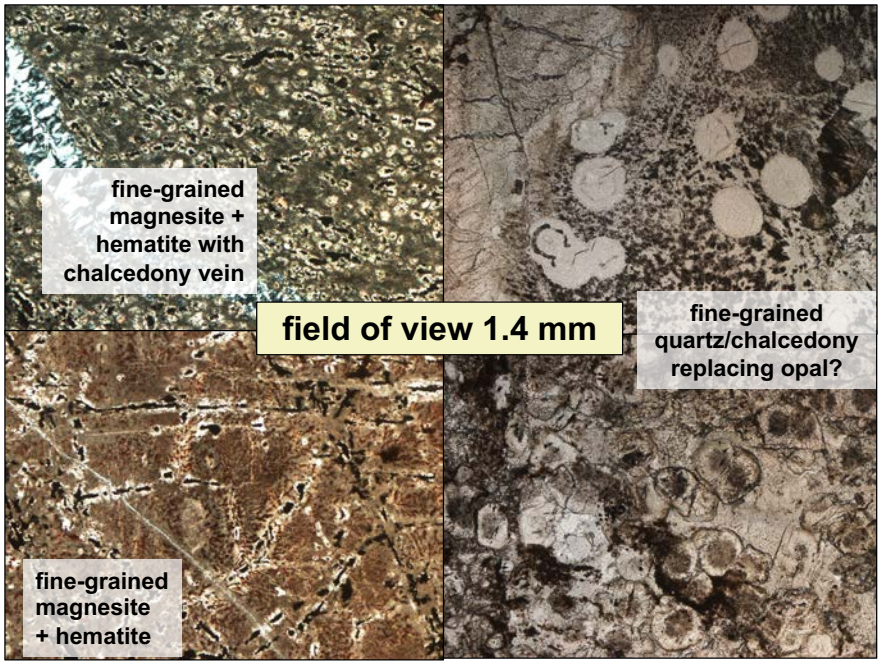

Figure 8: Plane light photomicrographs illustrating magnesite ovoids in a matrix composed of magnesite, quartz, and subordinate hematite and Fe-oxyhydroxides, TS_BT1B_20Z-1_42-46, ~ 40 m depth (left top) and TS_BT1B_27Z-2_6-8.5, ~ 59 m depth (left bottom), and quartz spherulites with carbonate and hematite inclusions, in matrix of fine-grained quartz and hematite with subordinate, microscopic carbonates, TS_BT1B_60Z-1_12-17, ~140 m depth (right).

Among the Fe-oxide veins, some contain minor sulfide – generally not detected during core description – and amorphous, organic carbon compounds. The carbon compounds were first identified in core at the drill site, in the lowest listvenite band, as elongate lenses within transposed hematite veins parallel to the penetrative foliation, where they were described as “graphite”. Soft organic carbon compounds in these features appear to have been largely lost from sample surfaces during washing and handling of the core prior to shipboard observations and analyses, and again during fabrication of thin sections. However, Raman spectroscopy of small, armored relicts, in oxide veins and also in isolated, dark red spots that resemble relict spinel on the core face and rock slabs, reveals the presence of disordered, thermally immature carbonaceous material (Figure 9), some of which may retain a more ordered organic molecular structure. The carbonaceous materials we can still find, on freshly cut surfaces from the core interior, are commonly on the margins of microscopic chalcocite and covellite crystals, in one case also associated with copper sulfate (chalcanthite)

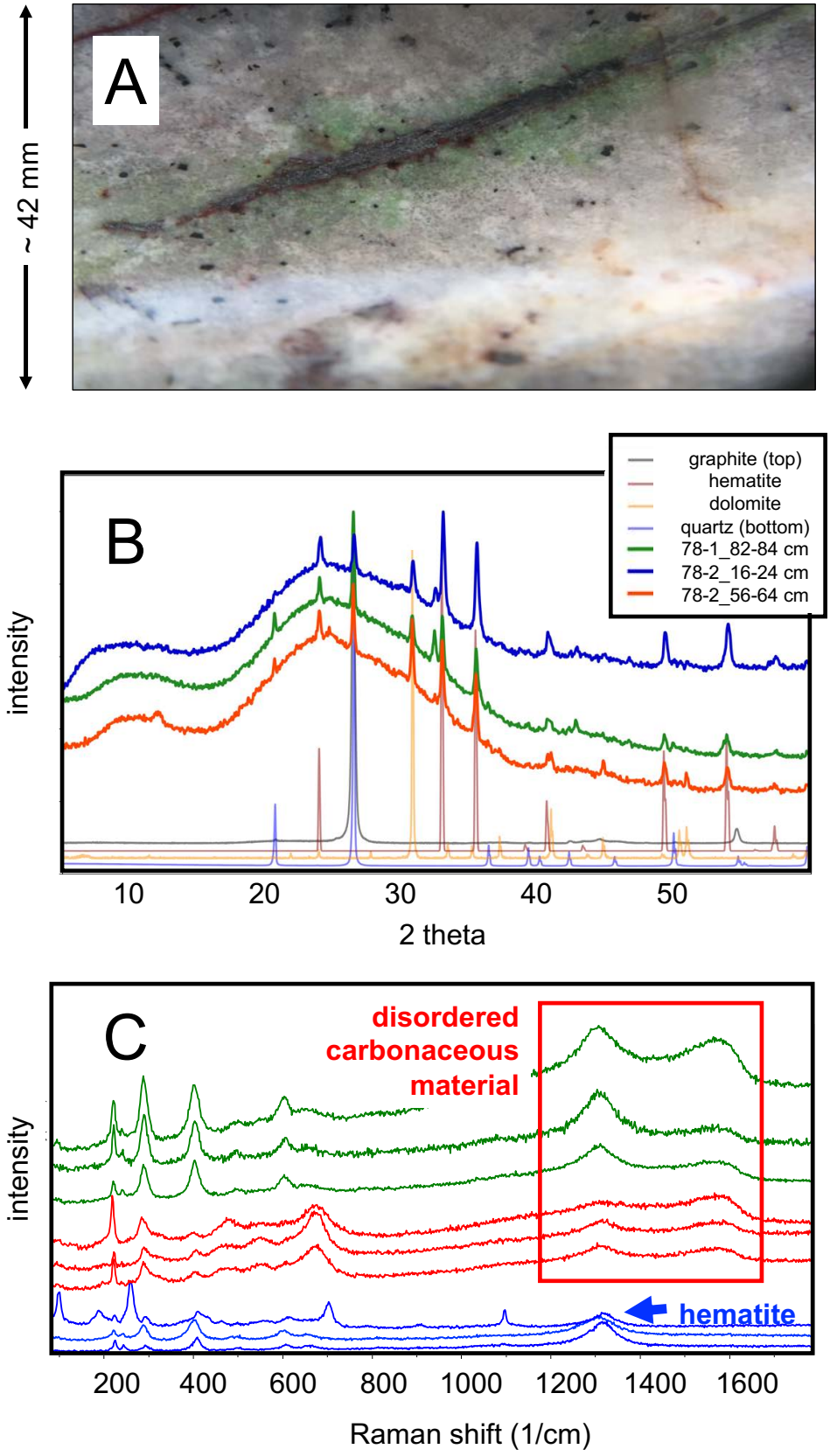
A
~ 42 mm
B
graphite (top)
hematite
dolomite
quartz (bottom)
78-1_82-84 cm
78-2_16-24 cm
78-2_56-64 cm
intensity
10
20
30
40
50
2 theta
C
disordered
carbonaceous
material
hematite
intensity
200
400
600
800
1000
1200
1400
1600
Raman shift (1/cm)

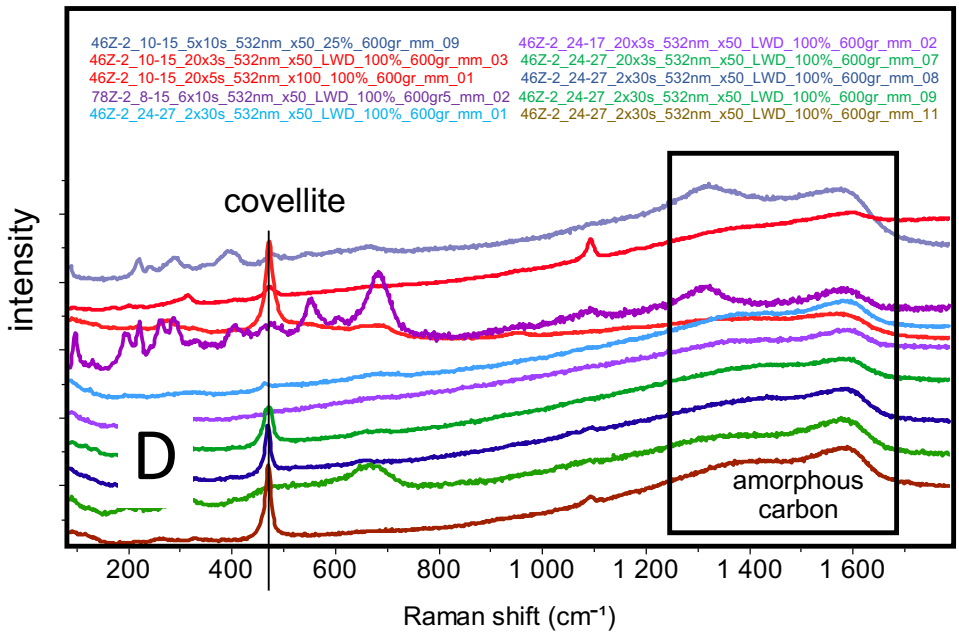

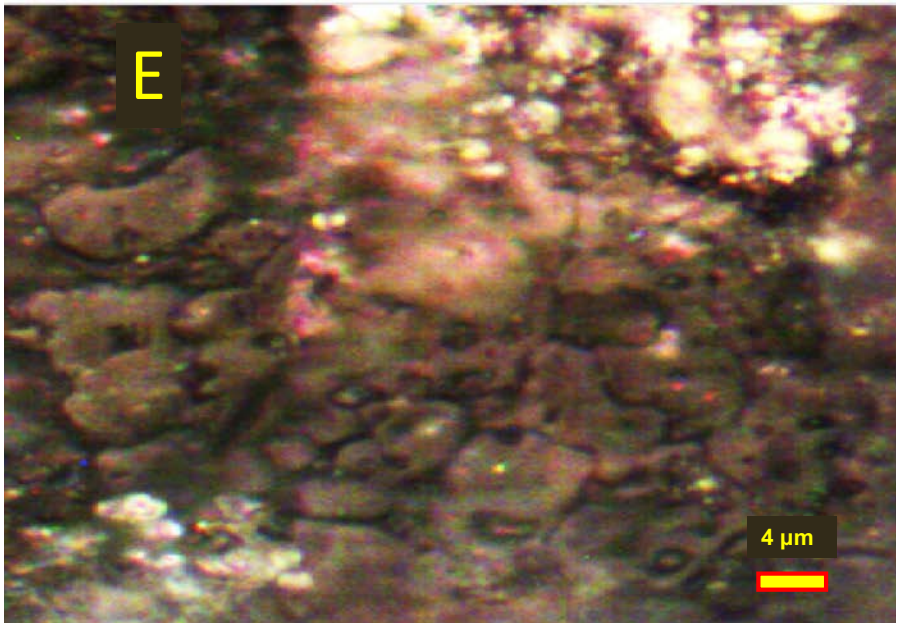

Figure 9: Carbonaceous material in drill core. A: Drill site photo of 1 to 2 mm vein of shiny, grey, soft material described as graphite on the drill site, in a vein rimmed with hematite. Field of view 5 cm wide, core 74Z-01, ~ 195 m depth. B: Shipboard XRD spectra of soft "graphite" powder extracted from veins with "graphite" + hematite, replacing Figure F43 in Kelemen et al. (2020b). Interpretation of these data is complicated by the similarity of the quartz and graphite peaks at ~ 26° 2Θ, but quartz also has a prominent peak at ~ 21°C which is absent from the blue spectrum for 78Z-02_16-24. C: Raman spectra of black material in samples BT1B_77Z-03_30-38 (blue), 78Z-02_8-15 (red) and 78Z-02_50-56 (green, ~ 192-198 m depth. Broad double peaks at wavenumbers of ~1350/cm and 1600/cm are indicative of disordered carbon compounds; no Raman spectra diagnostic of graphite were obtained. Many microscopic, soft, black domains contained hematite, with a single broad peak at ~1350/cm, instead of, or in addition to, disordered carbon compounds. D: Raman spectra of black material in samples BT1_44Z-02_10-15, BT1_78Z-02_8-15, and BT1_44Z-02_24-27, showing broad, double peaks indicative of disordered carbon compounds, some associated with covellite. Core 44Z ~ 98 m depth. E: dark grey copper sulfate "cow pies", spatially associated with brightly reflecting covellite, near amorphous carbon material, field of view ~ 100 microns, sample BT1_44Z-02_24-27. Data and images from core 44Z are from a 1 mm diameter black spot with a red rim in the interior of the core, exposed by the rock saw during sample preparation.

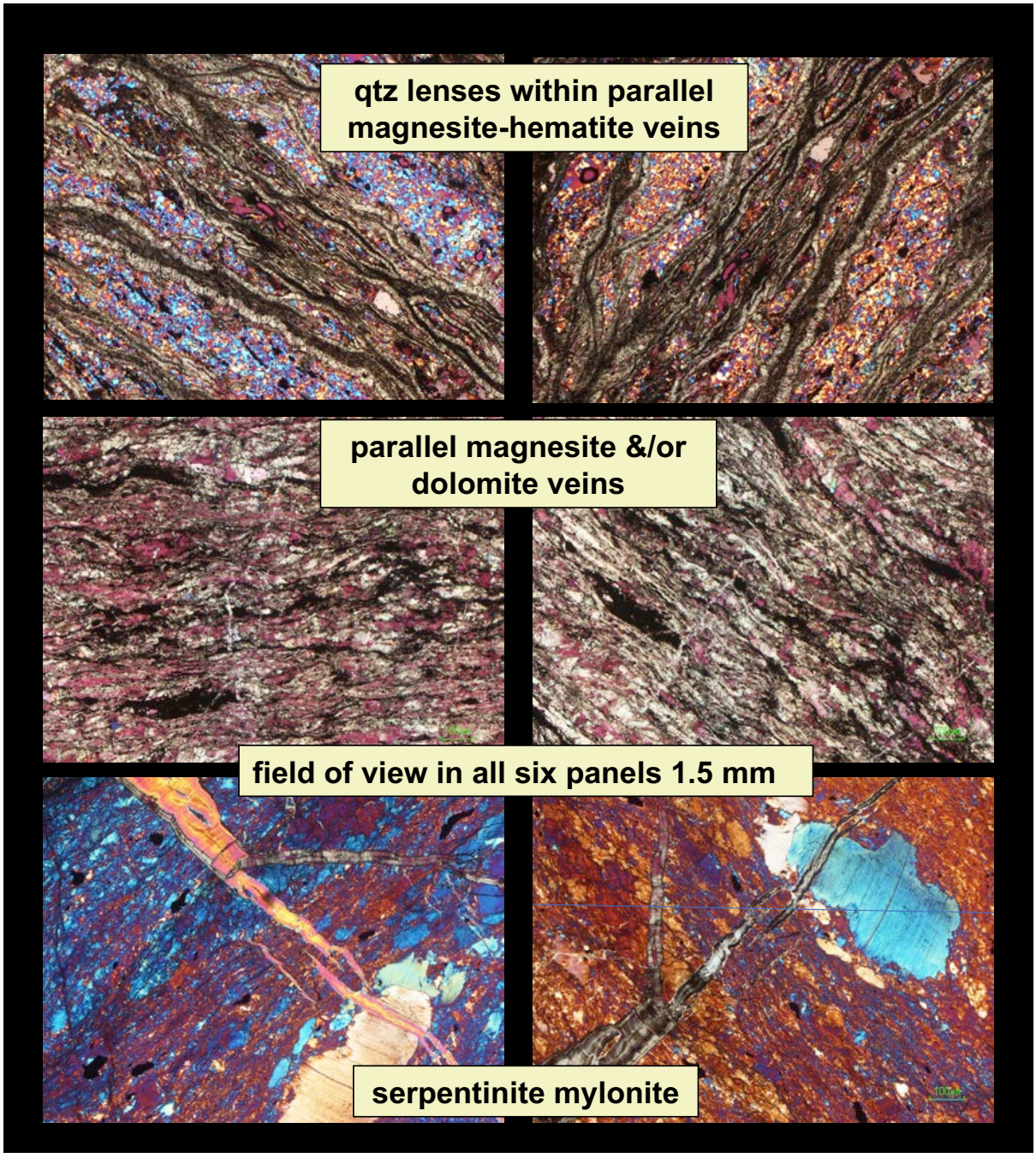

Figure 10: Examples of crystallographic preferred orientation (CPO) in localized zones in core from Hole BT1B. All images in cross-polarized light with quartz plate inserted. Images on right are of the same area as on left, but rotated 90° with respect to the polarizers. Areas showing optical continuity have a crystallographic preferred orientation. Top, TS_BT1B_31Z-4_12-14, ~ 65 m depth, quartz lenses within sub-parallel, anastomosing magnesite-hematite veins. Middle, TS_BT1B_78Z-2_34-38, ~ 195 m, thin section composed almost entirely of parallel magnesite and/or dolomite veins, with a CPO in the carbonates. Bottom, TS_BT1B_74Z-1_59-62, ~ 183 m, serpentinite mylonite, with a strong CPO in the fine-grained matrix, and visible, internal deformation in serpentine porphyroclasts.

4.5 Crystallographic preferred orientation of minerals

An overall preferred orientation of veins is not evident from structural data on the core scale, possibly due to differential rotation of core pieces. And, systematic measurements have not been made on the

outcrop scale. However, at the meter scale many core intervals contain textures indicative of ductile deformation (Figure 10). Some samples show a strong macroscopic foliation, defined by parallel (possibly transposed) veins enclosing elongate lenses of the fine-grained matrix, in textures commonly interpreted to form via boudinage during ductile deformation. In samples with a strong foliation defined by dozens of subparallel, early magnesite veins per 10 mm^2, intervening patches of fine-grained quartz commonly have a crystallographic preferred orientation (CPO). Some samples with a strong foliation defined by abundant, subparallel (tectonically transposed?) carbonate veins also have an optically evident, crystallographic preferred orientation in magnesite and/or dolomite. Similarly, some shear zones in serpentinite have an optically evident, strong shape- and crystallographic-preferred orientation of lizardite crystals, and contain deformed serpentine porphyroclasts.

4.6 Brittle deformation textures

A broad range of different breccias and cataclasites are observed in listvenites and in the metamorphic sole, in outcrop and in core. In turn these are cut by sharp faults – some associated with planar bands and branching veins of aphanitic ultracataclasite and/or pseudotachylite – and by late calcite veins. The nature and interpretation of cataclasites and faults observed in core from Hole BT1B are discussed in detail by Menzel et al. (2020).

4.7 Geochemical data

The bulk composition of core samples was measured in five different ways: (1) Major and minor element compositions of nine samples were measured by XRF at St. Andrews University. (2) Major and minor element compositions of 74 samples, including those previously analyzed at St. Andrews, were measured via XRF (both fusion and pressed pellets) onboard the Drilling Vessel Chikyu. (3) Major element compositions of the cut face of selected core sections were analyzed onboard using an XRF core scanner. (4) Trace element compositions of a few samples were analyzed onboard via ICP-MS. (5) Trace element compositions of 61 samples were analyzed via ICP-MS at the Université de Montpellier. These data, and subsequent analyses, are tabulated and described in Kelemen et al. (2020b) and Godard et al. (2021), so for brevity we simply refer readers to those other publications.

5. Discussion

5.1 Subduction zone setting of listvenite formation

On the basis of their structural observations west and northwest of the MoD Mountain area, and U/Pb formation or cooling ages from cross-cutting calcite veins, (60 ± 16 and 58 ± 6 Ma) Scharf et al. (2020) infer that listvenites in the Fanjah area postdate ophiolite emplacement, echoing the qualitative ideas of Stanger (1985) and Wilde et al. (2002). As noted in Sections 2.5 and 4.2, our

geochronological and field observations are inconsistent with this interpretation. The listvenite mineral isochron age of 97 ± 29 Ma (2σ) (Falk & Kelemen 2015) yields a 93% chance (1.5σ) that the listvenites formed before 75 Ma, while subduction beneath the ophiolite was still active, and a 97% chance that the listvenites formed before 68 Ma. Thus, the isochron data support listvenite formation during subduction, and show that the calcite veins cutting listvenite, dated by Scharf et al., postdate listvenite formation.

In this paper, our mapping and structural observations indicate an intact tectonic "stratigraphy" around the basal thrust of the ophiolite, encompassing the allocthanous Hawasina metasediments, overlain by the metamorphic sole, in turn overlain by Banded Unit dunites and harzburgites of the Samail ophiolite mantle section, with essentially horizontal lithologic contacts extending for kilometers. This is the stratigraphy created during subduction beneath the ophiolite, and – together with the isochron – it indicates that these units were juxtaposed during low angle thrusting along the subduction zone. In turn, all the listvenites in the MoD Mountain area are less than a kilometer away from the basal thrust, and have contacts with surrounding mantle peridotites and the metamorphic sole that are parallel to the basal thrust. All these data, taken together, indicate that the listvenites formed along and above the basal thrust of the ophiolite during subduction.

5.2 Faulting, deformation and veining after listvenite formation

(U,Th)/He cooling ages (Section 4.3) indicate that the region around MoD Mountain remained above the closure temperature for He diffusion in zircon, ~ 180°C (Reiners et al 2004), or were reheated above this temperature, during 30 to 60 million years after formation of the igneous crust in the ophiolite and peak metamorphism of the sole. Based on textural observations, it is clear that the breccias and cataclasites sampled in BT1B drill core postdate listvenite formation (Menzel et al 2020). Some may postdate ophiolite emplacement, and may be broadly related to Paleocene to Miocene uplift and extension during formation of the nearby Jebel Akdar and Saih Hatat domes. On the other hand, some could be related to deformation during subduction beneath the ophiolite. The long term persistence of temperatures above 180°C in this region renders it difficult to distinguish formation from cooling ages using (U,Th)/He data.

5.3 Temperature of listvenite formation

The temperatures of listvenite formation have been previously constrained using metamorphic phase equilibria, conventional oxygen isotope thermometry, and clumped isotope analyses. Falk & Kelemen (2015) noted the presence of intergrown antigorite (serpentine) + quartz. in the reaction zone between listvenite and serpentinite on the west ridge of MoD Mountain (Figure 2). In some cases, these samples also contain talc. They used Thermocalc (Powell et al 1998), with thermodynamic data from Holland and Powell (2003, 1998), and similar methods using the thermodynamic data of Gottschalk (1997), to estimate that equilibrium coexistence of antigorite, quartz and talc occurs at 80 to 120°C,

796 depending on the choice and uncertainty of thermodynamic parameters for the minerals, and the
797 (poorly known) pressure at which these assemblages crystallized. For this paper, we obtained similar
798 using Perple_X (https://www.perplex.ethz.ch/) (Connolly 1990, Connolly 2005, Connolly 2009) and
799 mineral properties from Holland and Powell.
800
801 In contrast, calculations using the Deep Earth Water (DEW) model (Huang & Sverjensky 2019,
802 Sverjensky et al 2014) and the extended Helgeson-Kirkham-Flowers (HKF) aqueous equation of state
803 (Shock et al 1992, Shock et al 1997) do not predict equilibrium coexistence of antigorite + quartz
804 above 15°C. Since antigorite-quartz intergrowths indicate coeval crystallization of both phases, in
805 rocks that formed at > 80°C, we presume that these latter results stem from incorrect extrapolation of
806 thermodynamic data to low temperature.
807
808 Leaving the DEW results aside, the other temperature estimates based on co-existing antigorite +
809 quartz are broadly consistent with temperature estimates based on $\delta^{18}O$ in quartz and carbonate
810 minerals in the listvenite, assuming that fluid $\delta^{18}O$ was similar to seawater, and with clumped isotope
811 analyses of magnesite and dolomite yielding temperatures of 80 to 130°C for listvenite samples (Falk
812 & Kelemen 2015). Observation of quartz spherulites in listvenite, possibly reflecting devitrification of
813 opal, also suggests that listvenite formation occurred in this "low temperature" regime, at ~ 150°C or
814 less, in the presence of aqueous fluid.
815

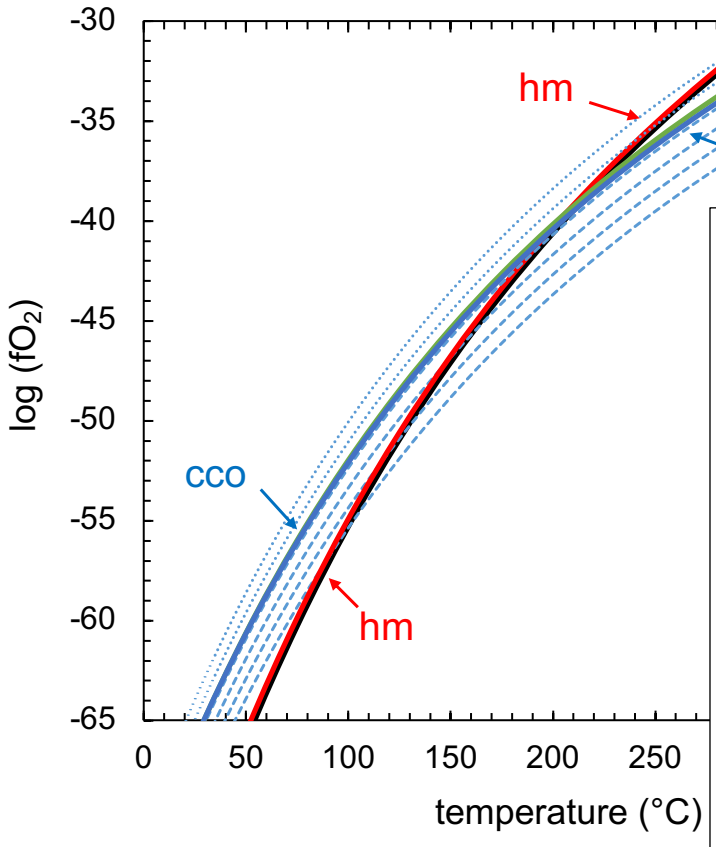

Figure 11: Diagram illustrating temperature and oxygen fugacity for the well-known oxygen buffers, hematite-magnetite (hm, $6Fe_2O_3 = 4Fe_3O_4 + O_2$) and graphite-carbon dioxide (cco, $C + O_2 = CO_2$). Graphite and amorphous carbon compounds are stable below the cco curves, while hematite is stable above the hm curve. hm curves are solid red (1 GPa) and black (0.2 GPa). cc curves are solid green (1 GPa) and blue (0.2 GPa). Dashed blue curves are for cco at 0.2 GPa total pressure, with $P(CO_2)$ = 0.1, 0.01, 0.001 and 0.0001 GPa from left to right. Dotted blue curves are for cco at 0.2 GPa total pressure = $P(CO_2)$, with a reduced activity of graphite (i.e., amorphous carbon compounds) 0.01 and 0.1 from left to right.

816
817

Here we show that veins of intergrown amorphous carbon compounds and hematite sampled in the core also must have formed below ~ 200°C (Figure 11). The observation of "reduced" hydrocarbon species intergrown with oxidized iron minerals in veins may seem surprising at first, but they are mutually stable at low temperature due to the stronger temperature dependence of the iron oxidation state, compared to the carbon oxidation state. Above ~ 200°C, reduced, organic carbon compounds and oxidized iron minerals such as hematite cannot coexist at the same oxygen fugacity, but they can crystallize together at moderate oxygen fugacities below ~ 200°C. We've found that this result is robust across all available sets of internally consistent thermodynamic data, and in the pressure range from 0.2 to 1.0 GPa.

Fourteen more recent clumped isotope analyses for listvenites and carbonate-bearing serpentinites from BT1B core yield an average temperature of 147±58°C (1σ). Ten of the 14 temperature estimates lie within the 1σ range, whereas two are lower (45±5 and 52±8°C) and the two least precise estimates are higher (227±52 and 247±52°C) (Beinlich et al 2020). Though a few MoD Mtn listvenites might have formed at temperatures greater than 200°C, such temperatures are too high for crystallization of intergrown amorphous carbon + hematite, they are too high for crystallization of intergrown antigorite + quartz, and they are too high for crystallization of opal. Also, carbonation of peridotite above ~150°C would form abundant talc + magnesite, whereas talc is absent in most MoD Mountain listvenites, and rare in serpentinite-listvenite contact zones that are gradational over a few meters (Falk & Kelemen 2015, Kelemen et al 2020b).

The range in temperature estimates based on phase equilibrium and clumped isotope ratios from the MoD Mountain listvenites may indicate that mineral assemblages in the listvenites and surrounding serpentinites formed gradually over a range of times and temperatures. In addition, some of the clumped isotope data may record closure temperatures during cooling, rather than the peak temperature at which the MoD Mountain listvenites first crystallized, as proposed for clumped isotope data from fine-grained 10-meter scale magnesite veins in California (Garcia del Real et al 2016). Alternatively, since the highest clumped isotope temperatures from Beinlich et al. are also the most imprecise estimates, perhaps they result from analytical uncertainties or disequilibrium effects. When the 14 clumped isotope temperatures from Beinlich et al. are combined with the 31 older clumped isotope temperatures from Falk and Kelemen, the full data set yields an average of 100 ± 46°C (1σ), with the highest temperatures from Beinlich et al. falling outside the 2.5σ (99% probability) range.

5.4 Depth of listvenite formation

The depth of listvenite formation is difficult to constrain. As noted in Section 2.4, published work on the metamorphic sole beneath the Samail ophiolite reports peak temperatures up to 700 to 900°C at pressures ranging from 200 to 1400 MPa, indicative of anomalously hot subduction zone conditions. Common peak pressure estimates, ~ 1200 MPa, indicate depths exceeding the structural thickness of

the ophiolite. Thus, either (1) the published range of pressure estimates for the metamorphic sole is the result of uncertainty rather than true variation in depth, and/or (2) the lower few km of the ophiolite mantle section has undergone thinning in some places, and/or (3) the lenses of the metamorphic sole recording the highest pressures migrated upward with respect to the overlying peridotite, and/or (4) some mineral equilibria record tectonic overpressures rather than lithostatic loads. Also, we infer from Sr isotope data that the fluids that formed the listvenites were not derived from the metamorphic sole (Section 5.6, below, and de Obeso et al 2021a). For all these reasons, it is unclear whether the metamorphic pressures inferred for the sole constrain the depth of listvenite formation. However, temperatures and pressures recorded by the sole do provide a window into the thermal evolution of subduction beneath the ophiolite before and during listvenite formation.

Initiation of subduction, during formation of the metamorphic sole, involved thrusting of a hot mantle wedge over newly formed, hot basaltic crust. Over time, subduction of progressively older oceanic crust and – eventually – the pelagic sediments of the Hawasina Formation would have caused cooling of the subduction zone as it evolved toward a steady state geotherm. A few clumped isotope analyses on calcite in sediments beneath the ophiolite and the metamorphic sole on MoD Mountain yield temperatures of 150 to 200°C (Falk & Kelemen 2015). It is possible that these were peak temperatures during diagenesis of the sediments along a late, steady state subduction geotherm at the pressure and depth recorded by the metamorphic sole in core from Hole BT1B, 800 -1200 MPa, or about 25 to 40 km.

In turn, even lower temperatures for most listvenite samples may record continued, isobaric cooling of rocks flanking the subduction zone. Temperatures of 100 to 200°C at depths of 25 to 40 km are inferred for fore-arc regions above subduction zones from heat flow data (reviewed in Peacock 1996) predicted for steady state, oceanic subduction geotherms in numerical models (e.g., Peacock 1996, Peacock et al 2005, Syracuse et al 2010), including those recently modeled by Van Keken et al. (2019), and lie within the cold end of the range of PT conditions recorded by subduction-related metamorphic rocks (Hacker 1996, Hacker 2006, Penniston-Dorland et al 2015). Such low temperatures at 25 to 40 km are rare or absent in other tectonic environments.

To summarize, it is possible that the sediments and the overlying mantle peridotites at the base of the ophiolite were juxtaposed by subduction at the leading edge of the mantle wedge, at a depth of 25 to 40 km, and that the MoD Mountain listvenites formed at these depths along a cold, steady state subduction geotherm. Alternatively, if the metamorphic sole has migrated updip with respect to the overlying peridotites, then the listvenites could have formed at lower pressures and shallower depths.

5.5 Composition of listvenite protolith and geochemical fluid additions

Given the abundance and variety of mineralogically simple veins, many of which are monomineralic, there is substantial compositional variation in listvenites at the millimeter to meter scale. This

variability extends to larger scales in some parts of the core. Nevertheless, remarkably enough, average MgO/SiO_2/FeO* (all Fe as FeO) ratios in the listvenites are very similar to those in average residual peridotites from the ophiolite (Figure 12), as discussed further by Okazaki et al. (Okazaki et al 2021). These oxides comprise more than 90% of the volatile-free bulk composition of the rock. These data suggest that there was little dissolution and export of major elements from the rocks during transformation of peridotite to serpentinite and then to listvenite as discussed further in Section 5.9.

On the other hand, serpentinites and listvenites record addition of tens of weight percent H_2O and CO_2 to the original bulk composition of mantle peridotite protoliths. In addition to CO_2, dolomite listvenites clearly record substantial addition of CaO, and – since CaO and Sr concentrations are strongly correlated – of Sr as well.

Although the shipboard data do not reveal systematic variation in the abundance of magnesite vs dolomite listvenites downhole, there is a clear change in the abundance of both Al and K, together with many other highly incompatible trace elements. Concentrations of these elements are relatively low above the serpentinite band at 80-100 m depth, and much higher below that band (Godard et al 2021, Kelemen et al 2020b).

Understanding the source for enrichment in these elements is complicated by uncertainty about their concentration in the peridotite protolith. As noted in Sections 2.3, 2.5 and 4.4, a “Banded Unit” of alternating dunite, harzburgite and lherzolite characterizes the base of the ophiolite mantle section in many regions. Some Banded Unit peridotites record high temperature geochemical “refertilization” by reaction of residual mantle peridotites with infiltrating melt or fluid at > 800°C, with addition of calcic pyroxene and Mg-rich hornblende. This produced enrichment in CaO and Al_2O_3 to levels well above those in typical residual mantle peridotites in the Samail ophiolite (Godard et al 2000, Hanghoj et al 2010, Monnier et al 2006). Indeed, four out of six harzburgite samples from the Banded Unit on MoD Mountain have Ca and Al contents outside the 1σ range of variability in residual mantle peridotite in the ophiolite (Falk & Kelemen 2015, Godard et al 2021, Kelemen et al 2020c).

The listvenites below 100 meters depth in core from Hole BT1B have trace element ratios that are distinct from typical peridotites, but characteristic of the Banded Unit (Figure 12 and Godard et al 2021), as shown in Figure 13. In particular, middle to heavy rare earth element ratios in the Banded Unit, and in the listvenites, are high compared to typical Samail peridotites. Such enrichment in middle rare earth elements is commonly associated with the presence of igneous hornblende in peridotites. Thus, the listvenites probably inherited these characteristics from the enriched, Banded Unit protolith.

On the other hand, it is clear that most listvenites have higher Sr concentrations than typical Samail ophiolite peridotites *and* the Banded Unit (de Obeso et al 2021a). Instead, Sr and Ca were added during low temperature alteration, along with H_2O and CO_2. These topics are discussed further by Godard et al. (2021).

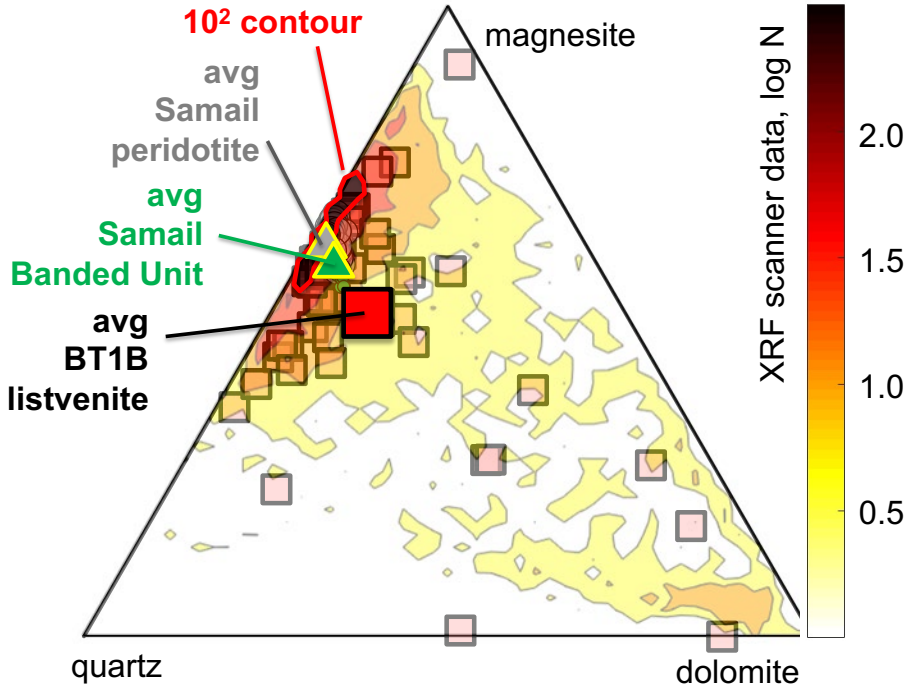

Figure 12: Ternary diagram illustrating volume proportions of quartz, magnesite and dolomite, projected from hematite, calculated from whole rock compositions, for Samail mantle peridotites (average in grey triangle, data as *large, grey open circles, barely visible beneath the averages and the 10^2 contour area,* Godard et al. 2000;Monnier et al. 2006;Hanghoj et al. 2010}*, Banded Unit peridotites near the base of the Samail ophiolite mantle section (small, green open circles, barely visible, Falk & Kelemen 2015, Khedr et al 2013, Khedr et al 2014, Takazawa et al 2003), and listvenites from Hole BT1B and MoD Mtn (open squares, Falk & Kelemen 2015, Kelemen et al 2020b), superimposed on contoured histogram of mineral proportions from shipboard XRF scanner data. Contour interval $10^{½}$. Okazaki et al. (2021) provide more thorough interpretation of shipboard XRF scanner data plus X-Ray Computed Tomography data on the whole core. Average listvenite, Banded Unit and Samail mantle peridotite compositions are provided in Supplementary Table 2.*

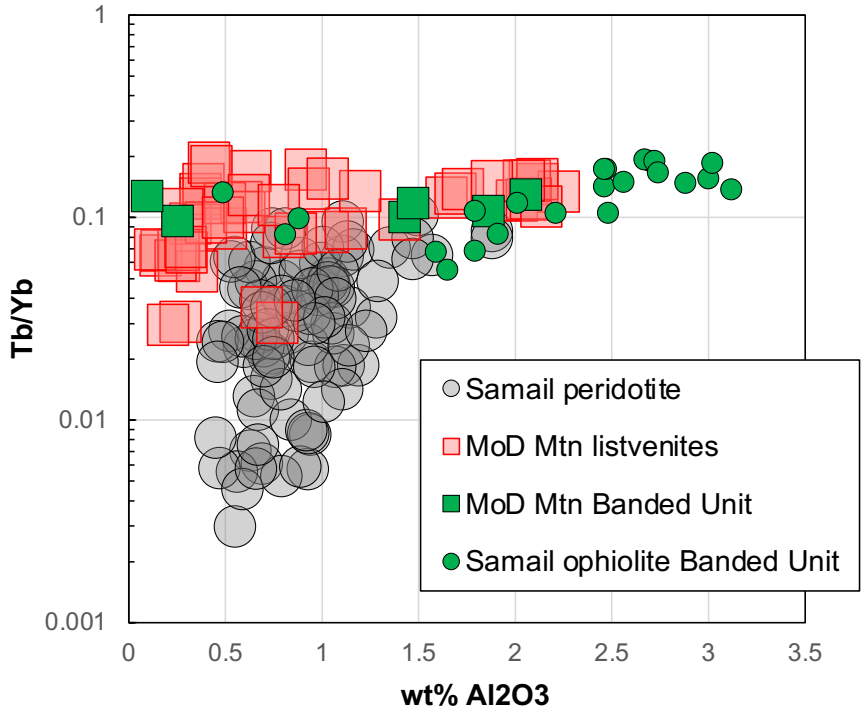

Figure 13: Wt% Al_2O_3 versus Tb/Yb ratios in bulk rock compositions of MoD Mtn listvenites (open squares, Falk & Kelemen 2015, Godard et al 2021, Kelemen et al 2020b), and MoD Mountain peridotites that host listvenites (green squares, Falk & Kelemen 2015, Godard et al 2021), compared to typical Samail mantle peridotites (grey open circles, Godard et al 2000, Hanghoj et al 2010, Monnier et al 2006), and Banded Unit peridotites from the base of the ophiolite (Khedr et al 2013, Khedr et al 2014, Takazawa et al 2003).

5.6 Source of fluid for listvenite formation

Present day Sr isotope ratios in listvenites and serpentinites from MoD Mtn range from ~ 0.708 to 0.715 (de Obeso et al 2021a, Falk & Kelemen 2015). Using current Rb/Sr contents in these samples, age corrected $^{87}Sr/^{86}Sr$ ratios at 96 Ma range from ~ 0.708 to 0.714, much higher than the range of Sr ratios in Samail ophiolite peridotites (0.703 to 0.707, Benoit et al 1999, Gerbert-Gaillard 2002, Gregory & Taylor Jr 1981, Lanphere et al 1981, McCulloch et al 1980, McCulloch et al 1981), the range in Late Cretaceous to modern seawater (~ 0.7075 to 0.7081), or the range in peridotite-hosted ground water in the Samail ophiolite (~0.7065 to 0.7092, Weyhenmeyer 2000). Thus, the Sr-, Ca- and CO_2-rich fluid(s) that modified the mantle overlying the basal thrust of the ophiolite had relatively high $^{87}Sr/^{86}Sr$ ratios compared to fresh, residual mantle peridotites.

Initially, we expected that the metamorphic sole, as sampled by core from Hole BT1B, might be the source of fluids that formed listvenites in overlying peridotites, or at least might be analogous to the source of these fluids. However, this is not consistent with the Sr isotope data on the sole in core from Hole BT1B. Measured and age-corrected Sr isotope ratios in the metamorphic sole are consistently lower than corresponding ratios in the listvenites (de Obeso et al 2021a).

Instead, pelagic, clastic units of the underlying Hawasina sedimentary rocks have measured and age-corrected Sr isotope ratios that span the same range as those in the listvenites (de Obeso et al 2021a). Thus, these sedimentary units in the Hawasina may be analogous to subducted sedimentary rocks that produced CO_2-bearing fluids which, in turn, formed the MoD Mountain listvenites. This is likely, despite the presence of C- and Sr-rich limestone and dolomite units with lower Sr isotope ratios in the Hawasina Formation, because devolatilization of clay and mica bearing, clastic metasediments produces abundant, CO_2-rich aqueous fluids, while limestone and marble remain relatively refractory at low to moderate temperature, subduction zone conditions (e.g., Kerrick & Connolly 2001, Stewart & Ague 2020).

Indeed, there is evidence for a deeply subducted component with terrigenous isotope characteristics – like those of the Hawasina clastic sedimentary rocks – elsewhere in the Samail ophiolite. A series of felsic intrusions in the sole, mantle and lower crust along the length of the ophiolite have low, age-corrected $^{143}Nd/^{144}Nd$ (and thus, presumably, high $^{87}Sr/^{86}Sr(t)$), attributed to melting of high-grade metasediment in the subduction zone below the ophiolite (Amri et al 2007, Briqueu et al 1991, Cox et al 1999, Haase et al 2016, Haase et al 2015, Lippard et al 1986, Rioux et al 2021a, Rioux et al 2013, Rioux et al 2021b, Rollinson 2015, Spencer et al 2017).

A complication is that the clastic units in the Hawasina formation have $\delta^{13}C$ less than -4 per mil, whereas listvenites have $\delta^{13}C$ > -3 per mil. These differences in carbon isotope ratios can be understood as the result of temperature dependent carbon isotope fractionation. As discussed in more detail in de Obeso et al. (2021a), at temperatures greater than ~ 300°C, dissolved CO_2 in

aqueous fluids has $\delta^{13}C$ higher than co-existing calcite and dolomite (Deines 2002, Horita 2014). At lower temperatures, calcite and dolomite have $\delta^{13}C$ higher than co-existing fluids. Dolomite and magnesite crystallized at relatively low temperature, from aqueous fluids that acquired their carbon isotope ratios during higher temperature devolatilization of Hawasina clastic sediment compositions, would have $\delta^{13}C$ in the range of 1.0 to -3.0‰, as observed in the MoD Mountain listvenites. In addition, low carbon solubilities in low temperature, low pressure aqueous fluids saturated in carbonate minerals in mineral assemblages similar to those in the Hawasina clastic sedimentary rocks (Figure 22 and associated text in Chapter 4, Falk 2014, Kelemen & Manning 2015) may be insufficient to produce the MoD Mountain listvenites (Falk & Kelemen 2015)de Obeso, 2021 #300}.

Based on the data and reasoning described in the previous paragraph, we hypothesize that subduction zone devolatilization at 400 to 600°C produced CO_2-rich aqueous fluids that then cooled and decompressed by flow up the subduction zone, and reacted with peridotite at less than 200°C to produce the MoD Mountain listvenites. To quantify this hypothesis, we made thermodynamic calculations with the compositions of solid reactants given in Supplementary Table 2, methods described in Section 3, and results outlined in Figures 14 and 15. As the source of fluid, we chose sample OM20-17, a pelitic end-member from among the Hawasina clastic sedimentary rocks analyzed by Falk & Kelemen (2015) and de Obeso et al. (2021a). As the peridotite reactant, we used an average Samail harzburgite composition calculated from published studies (Godard et al 2000, Hanghoj et al 2010, Monnier et al 2006).

Devolatilization of clastic Hawasina sediments, including OM20-17, is predicted to produce fluids with ~ 20,000 ppm dissolved C at ~ 400°C to ~ 600°C along subduction zone geotherms (Figure 14). Closed system decompression and cooling of fluid produced from OM20-17 to 100 to 300°C, and 0.5 to 1 GPa produced no significant change in the composition of this modeled fluid. (Modeling open system, reactive transport of this fluid, updip along a subduction zone geotherm, is beyond the scope of this paper, as is modeling the fate of subduction zone fluids that have more than 10 wt% CO2 – predicted for mixed siliciclastic-carbonate rocks (Figure 14) – as they cool and decompress).

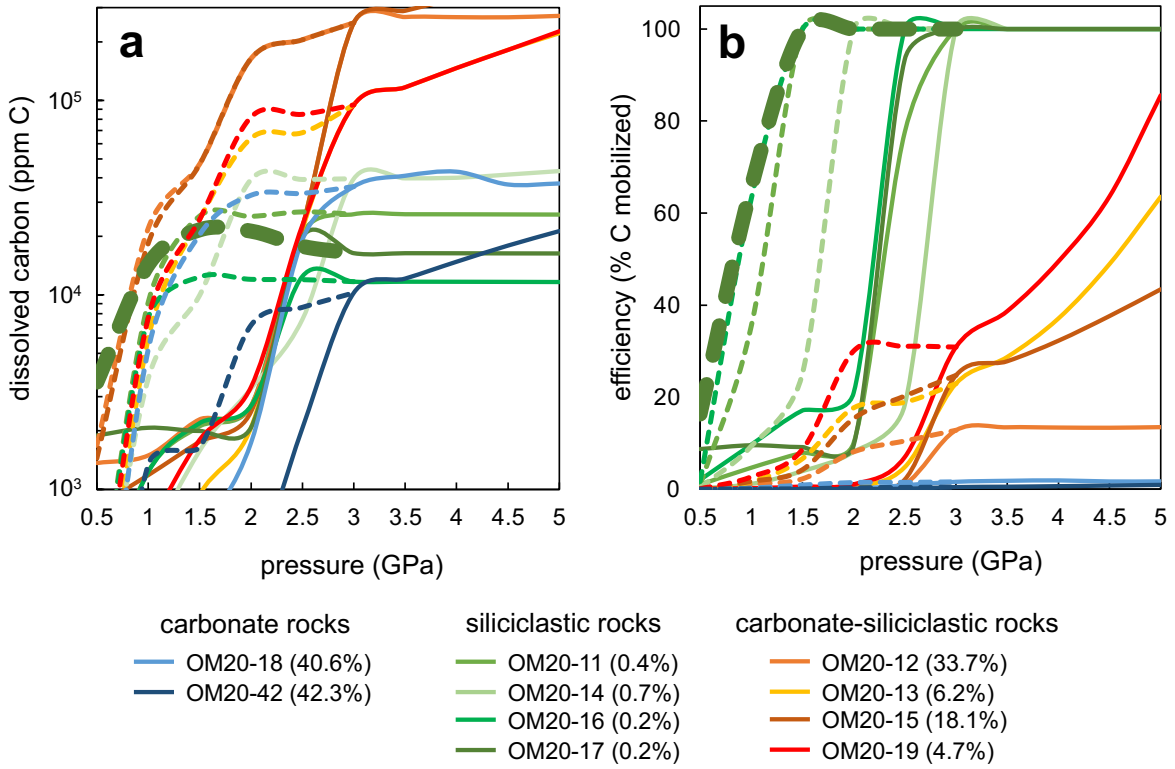

Figure 14: Calculated dissolved carbon concentrations at a water/rock ratio of 5% (a) and extent of carbon removal (b) for samples of Hawasina sediments in the MoD Mountain area (Supplementary Table 2 in de Obeso et al 2021a), evolving along cold (550°C at 2.5 GPa) and hot (500°C at 1.5 GPa) subduction geotherms. Solid curves are results for the average ("cold") subduction zone geotherm from Syracuse et al. (2010). Dashed curves follow a hot geotherm suggested by Penniston-Dorland et al. (2015). The initial carbon contents of the rocks (wt%, all carbon as CO_2) are given in the legend.

5.7 Listvenite formation

Reaction of the model fluid from OM20-17 with peridotite at 100-300°C and 0.5 to 1.0 GPa is predicted to produce mineral assemblages similar to those modeled by Klein and Garrido (2011): (1) Small masses of "birbirite" (silicified peridotite) at high water/rock ratios and/or low temperatures, through (2) moderate masses of listvenite and soapstone (talc-carbonate rocks) at moderate water/rock and temperature, to (3) relatively large masses of carbonate-bearing serpentinite at low water/rock ratios and/or high temperature (Figure 15). Predicted magnesite and quartz proportions correspond closely to observed proportions in MoD Mtn listvenites (Figure 12). Most of the PT conditions we modeled produced small amounts of hematite coexisting with magnesite and quartz, as observed. Predicted magnesite and siderite proportions correspond to a solid solution with ~ 8 wt% FeO, which is a few wt% higher than observed in MoD Mtn listvenites. Most modeled conditions produced dolomite in listvenite assemblages at water/rock ratios at water/rock ratios less than 10 (log water/rock = 1), consistent with the presence of relatively late, cross-cutting dolomite-bearing veins in the listvenites. Most model runs produce small amounts of kaolinite, and very limited proportions of muscovite, in listvenite mineral assemblages, consistent with the widespread presence of minor amounts of chromian white mica in MoD Mtn listvenites, and in listvenites worldwide. It is possible that addition of a thermodynamic model for fuchsite would yield stable white mica, rather than kaolinite,

over a wider range of temperature and water/rock ratios. Alternatively, perhaps some of the green sheet silicates in listvenites are chrome-bearing clays rather than true micas.

Thus, thermodynamic modeling suggests that the CO_2-bearing aqueous fluids that formed the MoD Mountain listvenites formed by metamorphic devolatilization in a subduction zone at > 400°C. These fluids then migrated updip to react with peridotite at the leading edge of the mantle wedge, probably at a depth less than 40 km. However, this is just a forward model, and there may be other possibilities.

Subhorizontal lenses of listvenite at MoD Mountain contain a cumulative mass of about 2 billion tons of CO_2 over a strike length of 2 km NS, and 5 km EW, corresponding to 1 million to 400,000 tons of CO_2 per m along strike. The allochthonous sedimentary units below the ophiolite are about 3 km thick. Within these, clastic units comprise at least half the section, and contain about 2300 ppm C, or 0.84 wt% CO_2 on average (de Obeso et al 2021a), yielding a total of about 35 tons CO_2 per m along strike, per m subducted. (As noted above, rocks composed mainly of calcite and/or dolomite in the subducting sedimentary section would be unlikely to contribute significant amounts of CO_2 to subduction fluids at temperatures less than 800°C). At subduction velocities of 0.05 to 0.1 m/year, 90% decarbonation of the clastic units in the Hawasina Formations with a density of 2.75 tons/m^3, at ~ 400-500°C would produce at least 1.7 to 3.5 tons of CO_2 per year per m of strike length. If most of this CO_2 reacted with peridotite at the depth and temperature of MoD Mtn listvenite formation, this could supply the observed mass of CO_2 at MoD Mountain in less than 600,000 years.

Most of the model results at different conditions predict precipitation of a few weight percent magnesite (and some dolomite) in the serpentinization domain. This is consistent with observation of carbonate veins in serpentinites from Hole BT1B, and with the hypothesis that formation of carbonate veins in the serpentinite zone preceded transformation of the serpentinite host rocks to listvenite (also see Figure 6 and associated text in Section 4.4,

The fluid temperatures, compositions and fluxes used in these calculations are different from the constraints used in some calculations by Falk & Kelemen (2015). In that previous work, we explored the possibility that CO_2 to form the listvenites was supplied over tens of millions of years, carried in 100 to 200°C fluids containing a few hundred ppm dissolved carbon, derived from pore fluids and/or dewatering of opal and clay minerals, from the Hawasina sedimentary rocks immediately below the site of listvenite formation at MoD Mountain. However, one of us (Falk!) insisted on mentioning the possibility that the CO_2 to form listvenites was derived from fluids formed deeper in the subduction zone, that migrated updip. We now prefer this latter hypothesis, for the reasons outlined above.

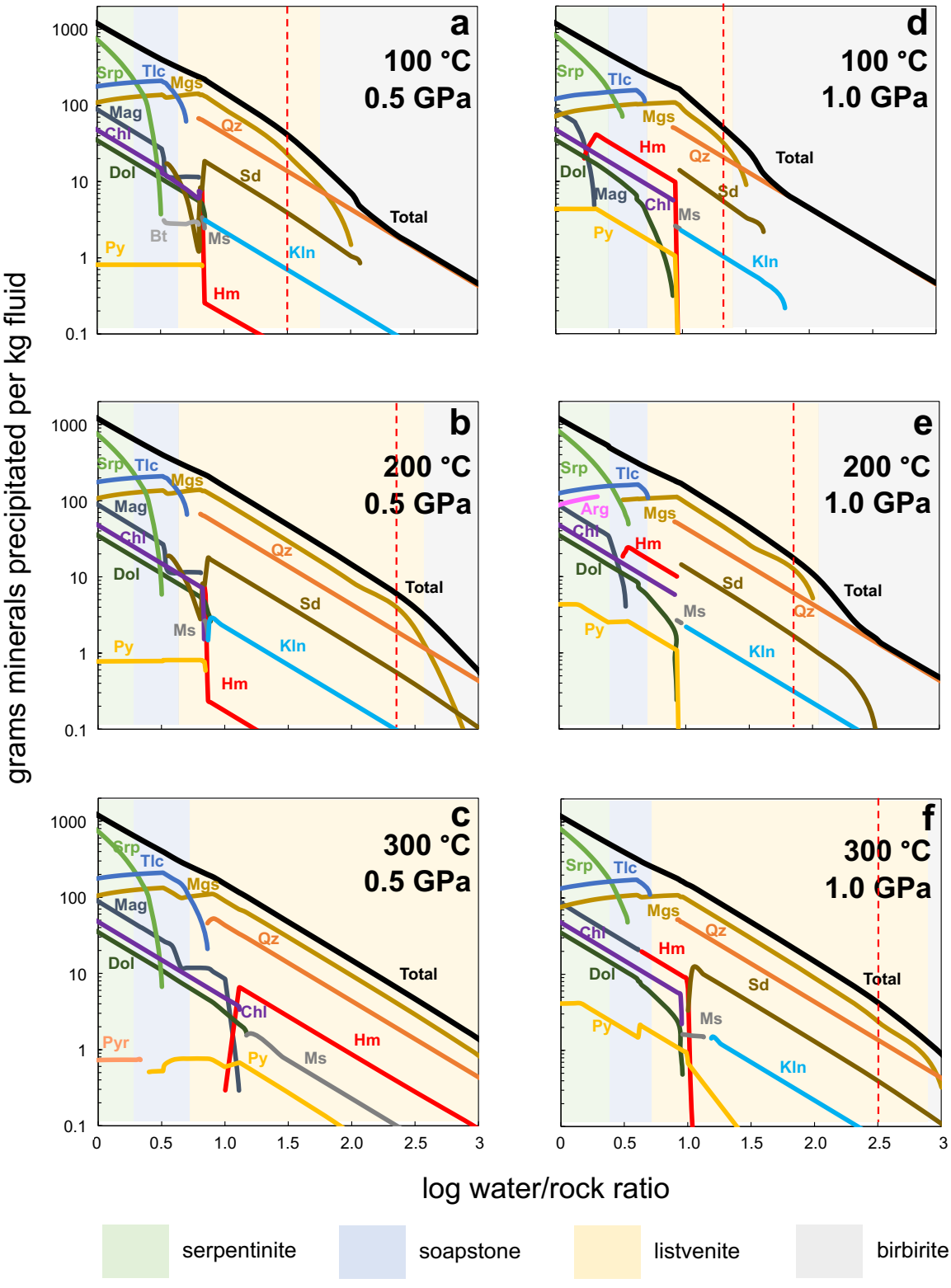

Figure 15: Results of thermodynamic reaction path models of reaction between fluids derived from devolatilization of Hawasina pelitic sedimentary rock sample OM20-17 (Section 5.6) and average Oman harzburgite. Mineral end-member abbreviations Qz quartz, Sd siderite, Mgs magnesite, Kln kaolinite, Ms muscovite, Dol dolomite, Chl chlorite, Py pyrite, Tlc talc, Srp serpentine (chrysotile), Pyr pyrrhotite. Red, vertical dashed line indicates where magnesite/quartz molar and volume proportions are ~ 2:1, as observed in magnesite listvenites from MoD Mtn (e.g., Figure 12).

Updip migration of fluids in a subduction zone has been predicted in some simplified dynamic models of fluid flow in a viscously deforming subduction zone with high permeability (Wilson et al 2014). However, the tendency of fluid buoyancy to drive vertical fluid flow may often dominate subduction zone fluid fluxes. Thus, formation of relatively shallow listvenites, like those at MoD Mountain, may be localized and unusual. Elsewhere, CO_2-bearing fluids may migrate vertically into overlying mantle peridotite at greater depth (e.g., Kelemen & Manning 2015). It is interesting to ponder how subduction zone CO_2 fluxes may be partitioned between these different transport and mineralization processes.

5.8 Multiple reaction fronts

The thermodynamic models presented in Sections 5.6 and 5.7 provide a starting point for understanding "chromatographic effects" during transformation of peridotite to serpentinite. As can be seen in Figure 15, our reaction path models predict sharp fronts where serpentinite is replaced by soapstone, and then by listvenite. Talc-bearing, soapstone assemblages are predicted to crystallize in a limited range of conditions, consistent with the fact that talc is rare in core from Hole BT1B, and in hand specimens from MoD Mtn, where it is almost entirely restricted to narrow (~ 1 m scale) transition zones between listvenite and serpentinite. If we were to use different thermodynamic data, talc might be even less abundant, or absent in models at 100°C, because talc is predicted to be unstable below ~ 100°C with respect to antigorite + quartz when using mineral data from Holland and Powell or Gottschalk, together with the Redlich-Kwong equation of state for H_2O- CO_2 fluids as modified by Kerrick and Jacobs (1981) and by Holland and Powell (2003).

In the model results presented in Figure 15, with reaction progress increasing from high fluid/rock ratios on the right to low fluid/rock ratios on the left, magnesite + quartz and magnesite + talc become unstable with respect to serpentine as dissolved carbon in the fluid is exhausted. Because carbon is a minor constituent of aqueous fluid, but a major component of the listvenite assemblage, exhaustion of dissolved carbon is predicted to occur at a fluid/rock ratio much greater than 1 (log fluid/rock > 0). Of course, because aqueous fluid is composed mainly of H_2O, the potential for serpentinization of peridotite continues to much lower fluid/rock ratios.

Although we cannot model it, we can also predict that – in the presence of pervasive fluid flow on the grain scale – there could also be a sharp front where serpentine replaces olivine at water/rock ratios less than one. Thermodynamic calculations for simplified olivine serpentinization by Kelemen et al. (2020a) indicate that olivine + H_2O would be stable with respect to serpentine at 100°C and a partial pressure of ~ 10^{-2} bars, and at 200°C and P(H_2O) ~ 1 bar. While these conditions cannot be modeled using EQ3/6, we can anticipate that low partial pressures of H_2O – much lower than lithostatic pressures – are produced along grain boundaries and near the tips of incipient fractures and veins, especially where fluid has been almost completely consumed by peridotite hydration reactions. Under these conditions, there could be a sharp front where serpentine (at higher fluid pressures) becomes stable relative to olivine (at lower fluid pressure).

Throughout the mantle section of the Samail ophiolite, residual mantle peridotites commonly contain about 50 to 80% serpentine, as inferred from the fact that bulk rock analyses yield loss on ignition (mostly, H_2O) of 8 to 10 wt% as compared to 13 to 16 wt% H_2O in completely serpentinized, Mg end-member harzburgite and dunites. These partially serpentinized peridotites commonly show a “mesh texture”, with relict olivine and pyroxene “cores” transected by a “mesh” of cross-cutting serpentine veins – typically 10 to 100 microns apart (Francis 1956, Green 1961, Green 1964, Raleigh & Paterson 1965). In some regions within the Samail ophiolite, particularly areas of relatively subdued topography that have undergone extensive, penetrative weathering, relict mantle minerals in the mesh cores are completely replaced by serpentine (e.g., OmanDP Sites BA1, BA2, BA3 and BA4, Kelemen et al 2021, Kelemen et al 2020c). However, along the steep canyons and narrow ridges that are typical of outcrops in the mantle section of the ophiolite, subject to relatively rapid erosion, the pervasive presence of the serpentine vein mesh surrounding relict mantle minerals attests to relatively rapid fluid transport in fractures and veins, compared to slow transport of H_2O into the mesh cores by diffusion and/or imbibition.

In contrast, as noted above, the serpentinites sampled in core from Hole BT1B contain no relict olivine or orthopyroxene, though pyroxene pseudomorphs (“bastites”) are evident. A zone of 100% serpentinized peridotites a few meters thick was sampled by Falk & Kelemen (2015) in a transect across a listvenite-peridotite contact on the watershed ridge east of the summit MoD Mountain. Outside this zone, samples of peridotite had compositions and textures typical of partially serpentinized residual mantle peridotites throughout the ophiolite. Based on these observations, we infer that there is a 100% serpentinite zone a few meters thick, with sharp fronts – less than a meter thick, between serpentinte and listvenite on one side, and between partially and completely serpentinized peridotite on the other side.

5.9 Volume change during listvenite formation

The likely volume change during fluid-rock reactions has long been debated. Whereas Coleman & Keith (1971) proposed that serpentinization involved simple addition of H_2O to peridotite, with no significant change in the volatile-free solid composition, Carmichael (1987), Nahon & Merino (1987), and Fletcher & Merino (2001) argued that such reactions take place at nearly constant volume, with addition of some components balanced by dissolution and export of others. Fletcher & Merino provided quantitative calculations to support this hypothesis. Where a fluid that is super-saturated in a new mineral phase, A, starts to crystallize A within a host mineral B that is initially in equilibrium with fluid, expansion of B around A leads to an increase in local effective stress. In turn, because chemical potential is proportional to the mean stress, this reduces supersaturation in A and leads to undersaturation in B. This process continues, with very small volume changes, until the rate of crystallization of A becomes equal to the rate of dissolution of B, at a steady state stress.

Using the methodology of Fletcher and Merino (2001) and a saturation index of 2 (as they did), Kelemen and Hirth (2012) calculated that the steady state, effective stress during replacement of olivine with serpentine is ~ 40 MPa. However, because olivine is very far from equilibrium with water at low temperature, the saturation index for water reacting with olivine to form serpentine at 50 to 250°C and $P(H_2O)$ > 1 bar is close to 10^7, and the steady state, effective stress estimated using the method of Fletcher and Merino is ~ 800 MPa (Kelemen & Hirth 2012). Clearly, such a large differential stress cannot be sustained within most rocks, which will deform at a lower stress, before the steady state can be reached, either via ductile mechanisms (if reactions are slow and temperatures are high) or via fracture and frictional deformation (if reactions are fast and temperatures are low). The latter outcome is sometimes termed “reaction-induced cracking” (Jamtveit et al 2009, Rudge et al 2010) or “reaction-driven cracking” (Kelemen & Hirth 2012). Thus, while some workers still disagree over the extent of volume change in specific replacement processes, the approach of Fletcher and Merino nicely explains a continuum between nearly constant volume replacement of one mineral by another at high temperature, close-to-equilibrium conditions, and large volume changes accommodated by fractures and frictional sliding at low temperature, far-from-equilibrium conditions.

As noted in Section 5.5 , despite dramatic, local variability, the average major element composition of listvenites from MoD Mountain – in drill core and surface samples – is strikingly similar to the average composition of residual mantle harzburgites in the Samail ophiolite. Together, the concentrations of MgO, SiO_2 and FeO* (all Fe as FeO) account for more than 90% of the volatile-free bulk composition of listvenite samples. Thus, the fact that average Mg/Si/Fe ratios in the listvenites are almost identical to those in Samail peridotites suggests that either (1) large scale dissolution of the peridotite protoliths was nearly congruent, exporting dissolved, major elements in approximately their initial proportions, or (2) there was little dissolution and export of major elements in the protolith during addition of CO_2 to form listvenites, and addition of H_2O to form serpentinites.

Thermodynamic models, experimental data, and observations of natural rock samples strongly favor the second of these hypotheses. The solubility of silicate and Fe-oxide minerals in rock-buffered aqueous fluids at low temperature is too low to allow for large scale dissolution and export of major elements in open system, fluid-rock reactions. In turn, models of addition of CO_2 and/or H_2O to peridotites, predict very little removal of other species, togther with large increases in the mass and volume of the solid products of reaction. Birbirite formation may involve net volume and mass loss due to extensive dissolution of peridotite reactants at water/rock ratios greater than ~ 100. However, the models of listvenite formation illustrated in Figure 15 yield predicted mass and volume increases of 10 to 55 percent relative to an anhydrous, peridotite reactant, as illustrated in Figure 16. Similar results have been produced by thermodynamic models of serpentinization (volume increase of 40-60%, de Obeso & Kelemen 2018, Malvoisin 2015), experimental observation of closed system serpentinization (30-60%, Klein & Le Roux 2020) and analysis of microstructures in partially serpentinized peridotites formed in an open system (59±30 to 74±36%, Malvoisin et al 2020).

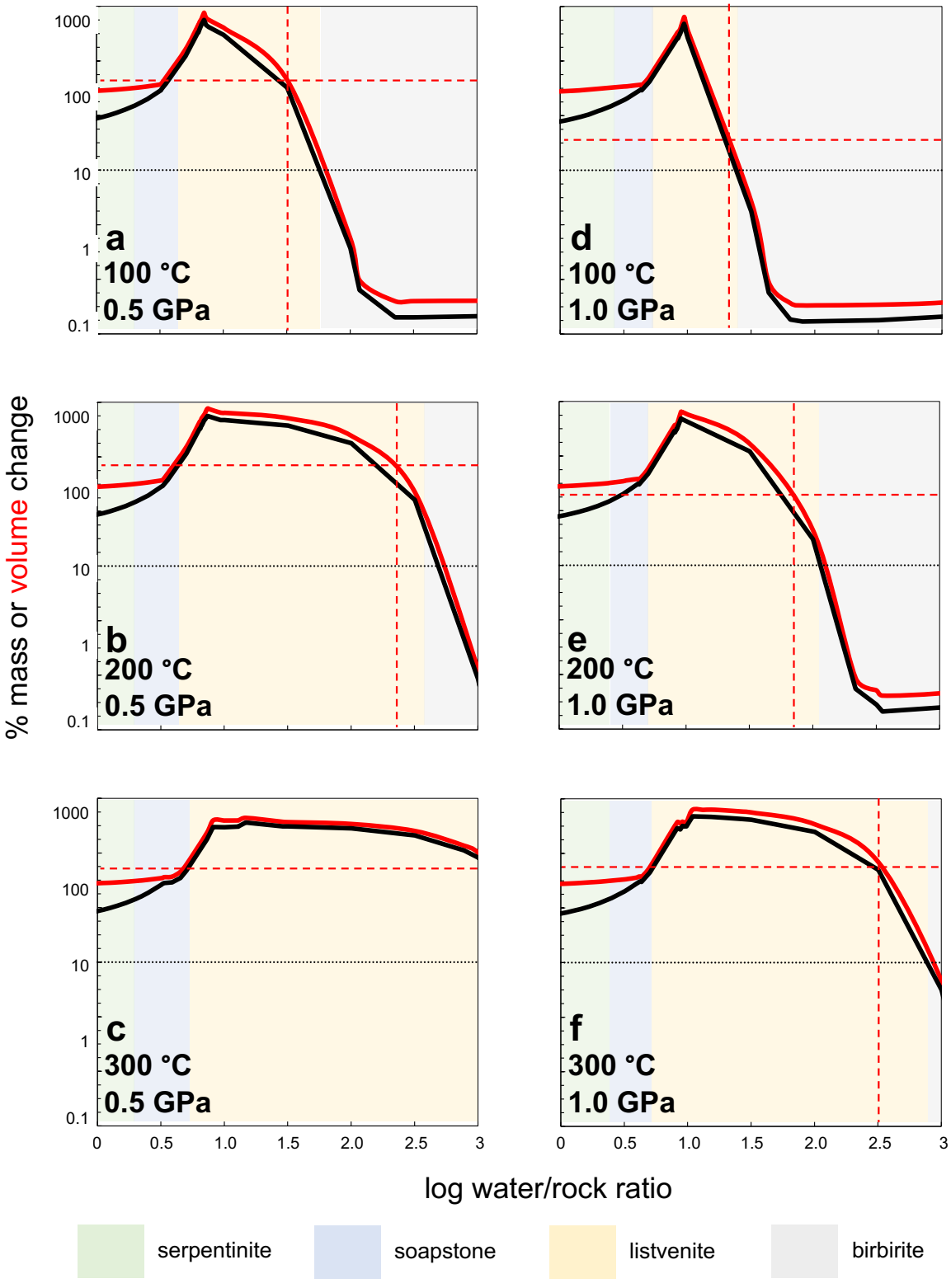

Figure 16: Calculated mass and volume change relative to an anhydrous peridotite, for the reaction path models illustrated in Figure 15. Dashed, vertical red lines indicate where molar and volume proportions of magnesite/quartz reach 2:1, as onserved in MoD Mtn listvenites (e.g., Figure 12). Dashed, horizontal line highlights the minimum increase in solid volume calculated for listvenite formation.

These modeled and observed volume changes approximate those resulting from simplified, Fe-free, stoichiometric reactions. Thus, hydration of olivine to form serpentine and brucite,

$$2Mg_2SiO_4 + 3H_2O = Mg_3Si_2O_5(OH)_4 + Mg(OH)_2, \quad (1)$$

and hydration of olivine + orthopyroxene to form serpentine,

$$Mg_2SiO_4 + MgSiO_3 + 2H_2O = Mg_3Si_2O_5(OH)_4, \quad (2)$$

can produce 52 and 63% increases in the solid volume, respectively. (Volume change calculated as 100% (product volume -reactant volume)/(reactant volume)). Direct carbonation of olivine

$$Mg_2SiO_4 + 2CO_2 = 2MgCO_3 + SiO_2, \quad (3)$$

and olivine + orthopyroxene,

$$Mg_2SiO_4 + MgSiO_3 + 3CO_2 = 3MgCO_3 + 2SiO_2, \quad (4)$$

can lead to 85% and 74% increases in the solid volume, respectively. And, carbonation of serpentine plus brucite

$$Mg_3Si_2O_5(OH)_4 + Mg(OH)_2 + 4CO_2 = 4MgCO_3 + 2SiO_2 + 3H_2O, \quad (5)$$

and serpentine alone

$$Mg_3Si_2O_5(OH)_4 + 3CO_2 = 3MgCO_3 + 2SiO_2 + 2H_2O, \quad (6)$$

both produce solid volume increases ~ 22%.

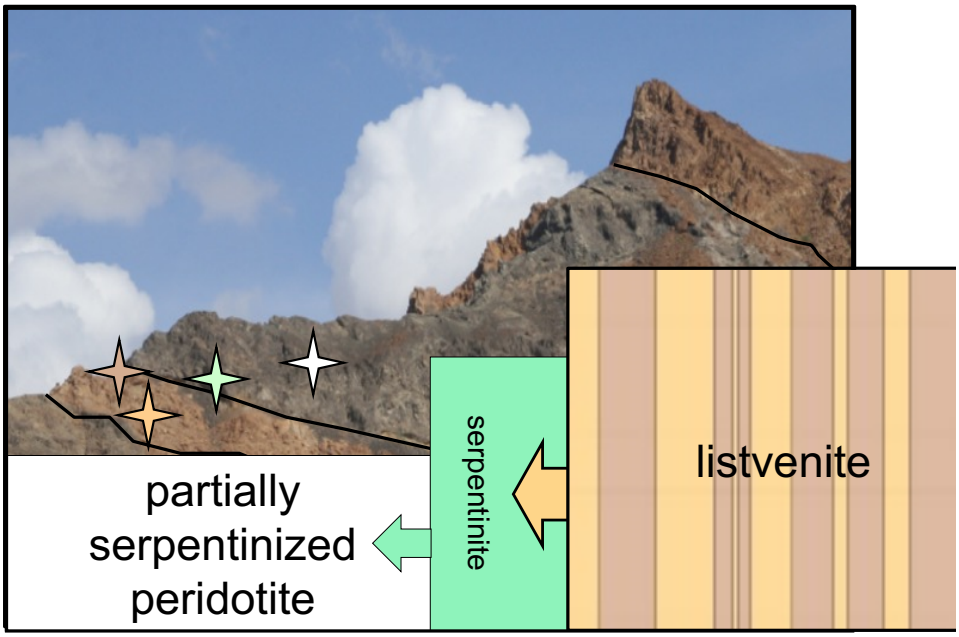

Figure 17: Schematic illustration of sequential volume changes during replacement of partially serpentinized peridotite by serpentinites and then replacement of serpentinites by listvenites. The height of the rectangles corresponds to the relative volumes, produced by reaction of CO2-bearing fluid with an initial, anhydrous peridotite. The tan and brown stripes in the "listvenite" represent alternations of different listvenite compositional bands. Stars on photo of the SW side of MoD Mtn illustrate position of listvenite, serpentinite and partially serpentinized peridotite samples (Falk & Kelemen 2015).

Because porosities in peridotite, serpentinite and listvenite rarely if ever exceed 5%, all of these solid volume changes must be accommodated mainly by expansion of the entire rock volume. It is interesting to speculate how much uplift – and/or lateral expansion – in forearc regions is caused by

hydration and carbonation of the mantle wedge. However, at the plate tectonic scale, the rates of reactions similar to those outlined in equations (1-6) are unknown. It is likely that the strains due to reaction are comparable to, or smaller than, other rates of deformation at convergent plate boundaries, rendering the effect of solid volume expansion difficult to detect at the regional scale.

Based on the considerations outlined in this section, it is likely that large increases in the solid volume occurred during formation of the MoD Mountain listvenites, and were accommodated mainly by reaction-driven cracking, frictional sliding along existing fractures, and/or reaction-assisted granular flow (Menzel et al 2021). The presence of abundant, antitaxial magnesite, magnesite-hematite, and Fe-oxide veins in both serpentinites and listvenites is qualitatively consistent with a reaction-driven cracking process. However, we have not identified any obvious strain markers that would allow a quantitative evaluation of this hypothesis using rock textures.

Building upon an idea from Hansen et al. (2005), the Shipboard Scientific Party developed the hypothesis that large volume increases due to hydration of olivine and pyroxene (reactions 1 & 2) may have initially formed fractures at (and beyond) a serpentinization front – not observed in drill core, but traversed by Falk & Kelemen (2015) – and these fractures were conduits for fluid flow and sites of localized deformation during the smaller volume changes due to carbonation of serpentinites (reactions 5 and 6) as schematically illustrated in Figure 17.

5.10 Low temperature ductile deformation in subduction zones

As noted above, the listvenites at MoD Mountain may have formed at depths of 25 to 40 km, at temperatures less 200°C, yielding low temperature “geotherms” of 5 to 8°C/km depth. Such small increases of temperature with depth are characteristic of the forearc above subduction zones (Peacock 1996). High fluid pressures at these depths may account for the somewhat surprising indications of low temperature, ductile deformation in core samples from Hole BT1B, based on the observed crystallographic preferred orientation (CPO) in quartz, magnesite and serpentine in core samples (Section 4.4, Figure 10).

Some of the fabrics illustrated in Figure 10 could be inherited. For example, in early formed, magnesite-hematite veins, magnesite forms parallel crystals, perpendicular to vein margins, with small misorientations between adjacent crystals. When these veins are parallel (because they form that way, or after they are transposed), this imparts a CPO to the sample, and may also give the impression that sub-grain boundaries are present, even if there was no deformation of magnesite crystals via dislocation creep. Similarly, quartz replacing opal may inherit a CPO, or a CPO may arise due to anisotropic stress during recrystallization, without substantial strain.

On the other hand, the serpentine mylonite illustrated in Figure 10 almost certainly records large strains due to distributed deformation along grain boundaries. Moreover, clear examples of ductile

deformation and shear zones with classical indictors of substantial strain indicate that ductile deformation was active during the initial stages of listvenite formation, perhaps assisted by positive feedback between weakening, due to reaction-induced recrystallization, and porosity enhancement due to deformation, as discussed by Menzel et al. (2021). An important role for ductile deformation in reaction zones at the top of subducting oceanic crust may help to explain why, in the relatively hot Cascadia and SW Japan subduction zones, there are very few earthquakes at the top of the subducting crust (Abers et al 2009, Abers et al 2013, Hirose et al 2008).

6. Conclusions

Observations of drill core of listvenite (completely carbonated peridotite), serpentinite, and subduction-related metamorphic rocks from OmanDP Hole BT1B provide constraints on temperature, depth, and deformation during mass transfer of H_2O and CO_2 from subducted sediments into overlying mantle peridotites at the leading edge of the mantle wedge. Listvenites, and a surrounding zone of serpentinite, formed at temperatures less than ~ 200°C and poorly constrained depths of 25 to 40 km. Serpentinization and carbonation involved reaction of partially serpentinized, residual mantle peridotite with CO_2-rich, aqueous fluids produced by devolatilization of subducting, clastic sediments analogous to the Hawasina formation, probably at 400 to 600°C. These fluids cooled as they were transported up the subduction zone to the site of listvenite formation.

Such processes could play a significant role in the global carbon cycle. Not all listvenites form above subduction zones. However, listvenites are found at and near the basal thrust in other ophiolites, worldwide (Akbulut et al 2006, Borojević Šoštarić et al 2014, Escayola et al 2009, Menzel et al 2018, Quesnel et al 2016, Quesnel et al 2013, Scarsi et al 2018, Sofiya et al 2017, Ulrich et al 2014). The leading edge of the mantle wedge – and subduction modified mantle that has later been incorporated into the continental mantle lithosphere – may be a globally important reservoir for carbon (Foley & Fischer 2017, Kelemen & Manning 2015, Li et al 2017, Scambelluri et al 2016)

During BT1B listvenite formation, total solid volume increased by tens of percent due to hydration followed by carbonation. While core and surface samples provide few direct constraints on the mechanism that accommodated this expansion, one hypothesis is that large volume changes during hydration of olivine and pyroxene along a serpentinization front caused large stresses and fractures that accommodated expansion via frictional sliding, and provided secondary porosity for the CO_2-rich fluids that transformed serpentinites to listvenites.

Based on observed crystallographic preferred orientation in quartz, magnesite and serpentine in macroscopically identified shear zones, it is inferred that ductile deformation of listvenite and serpentinite occurred under low temperature conditions at the base of the mantle wedge during subduction. Low temperature ductile deformation, coeval with serpentinization and listvenite formation, may have been facilitated by recrystallization associated with the hydration and carbon

mineralization processes, as discussed in more detail by Menzel et al. (Menzel et al 2021). Such a process could be active in subduction zones where the interface between subducting oceanic crust, sediments, and hanging wall peridotites is aseismic.

6. Author contributions

Kelemen and de Obeso conducted field mapping at MoD Mountain. de Obeso made new Sr and C isotopic analyses of listvenites, the metamorphic sole and the underlying sedimentary rocks, updating work by Falk & Kelemen (2015). Stockli carried out the reconnaissance (U,Th)/He analyses of zircons from the metamorphic sole and lower curst, using zircon separates samples provided by Rioux. Godard expertly led the BT1B geochemistry team onboard Drilling Vessel Chikyu, and then heroically continued with analyses at the Université de Montpellier on behalf of the Shipboard Scientific Party. Okazaki labored with Kelemen on the triangular histogram of shipboard XRF scanner data. Leong and de Obeso conducted the EQ3/6 thermodynamic modeling, in consultation with Kelemen. Working with his computer in 46°C weather on the drill site, Manning provided key insights into conditions for coexisting hematite and organic carbon compounds. Ellison supervised Kelemen's Raman spectroscopy analyses at the University of Colorado, Boulder, and offered essential advice and data interpretation. Kotowski led analysis of core from the metamorphic sole and shared her results. Urai led the structural geology team during core description onboard DV Chikyu, and is now advising Menzel, who is leading analysis and interpretation of microstructures. Hirth offered insights into potential mechanisms of low temperature, ductile deformation in subduction zones. Lafay and Beinlich provided valuable input on the drill site and as members of the Shipboard Scientific Party. Coggon (Project Manager) supervised drilling, core curation and logistics for this and all other OmanDP boreholes, together with Nehal Warsi (Site Geologist). Matter (Project Director), Teagle (ICDP Lead Investigator) and Sulaimani (Country Manager) worked tirelessly to ensure the success of the Oman Drilling Project. Harris, Kelemen, Michibayashi, and Takazawa served as Co-Chief Scientists onboard DV Chikyu during description of core from Hole BT1B. Kelemen (Chief Scientist) helped lead the project, had a few ideas, and took the lead in writing this manuscript.

7. Acknowledgements

Drilling and research in the Oman Drilling Project were supported by the Alfred P. Sloan Foundation (in association with the Deep Carbon Observatory, DCO), the International Continental scientific Drilling Program (ICDP), US National Science Foundation (NSF) Research Grant NSF-EAR-1516300, the Japanese Marine Science and Technology Center (JAMSTEC), grant number 16H06347 from the Japanese Society for the Promotion of Science (JSPS), the US National Aeronautics and Space Administration (NASA, including the Rock Powered Life NASA Astrobiology Institute (NNA15BB02A), the European Science Foundation, the German Science Foundation, the Swiss Science Foundation, and the International Ocean Discovery Program (aka International Ocean Drilling Program, IODP). Kelemen's research was also supported with funds from the Arthur D. Storke Chair at Columbia

University. In addition to the authors of this paper, a huge team contributed to the success of OmanDP, including drilling and core analyses at Hole BT1B. In Oman, a Project Supervisory Committee chaired by Dr. Said Al Habsi (Director General of Water Resources Assessment in the Ministry of Regional Municipalities and Water Resources), and including Prof. Sobhi Nasir at Sultan Qaboos University, Dr. Ali Al Rajhi, Director of the Geological Survey of Oman, and others, ensured that the project went forward smoothly in accordance with Omani requirements. At Petroleum Development Oman (PDO), Dr. Hamad Shuaili and Dr. Hisham Siyabi kindly facilitated storage of the archive half of all OmanDP core. We particularly thank Dr. Jay Miller and Dr. Brad Clement at IODP TAMU for making the online proceedings volume possible, and Shana Lewis, Rhonda Kappler, Jean Wulfson, Phil Rumford, Lorri Peters, Crystal Wolfe and Kenneth Sherar at IODP TAMU for editorial assistance in preparing the Proceedings of the Oman Drilling Project, more or less following IODP protocols in presenting the results of this decidedly non-standard ICDP project. We thank the technical staff onboard Drilling Vessel Chikyu for fantastic, efficient support and advice over four months in summers 2017 and 2018, especially Lena Maeda, Dr. Yusuke Kubo, and Dr. Chiaki Igarashi. Dr. Nobu Eguchi served as a patient, generous liaison between OmanDP, NSF and JAMSTEC. Core description onboard Chikyu would have been impossible without proactive support from JAMSTEC President Asahiko Taira and NSF Program Director Leonard Johnson. Similarly, we received essential assistance with borehole permitting from Professor Ali Al Bemani, Vice Chancellor of Sultan Qaboos University. On a different timescale, we are deeply indebted to His Majesty Sultan Qaboos bin Said Al Said for his open-door policy for scientific research in Oman, and to Professors Françoise Boudier, Bob Coleman, Cliff Hopson and Adolphe Nicolas for establishing the framework for modern studies of the Samail ophiolite.

Suggestions from Othmar Müntener, an anonymous reviewer, and Associate Editor John Lassiter led to substantial improvements of this paper.

Data Availability: Samples in Supplementary Table 1 have IGSN numbers and locations. Data in Supplementary Table 1 are in the process of being archived in the Geochron database (www.geochron.org). Figures 4, and 6 are compilations of images that are published at http://publications.iodp.org/other/Oman/OmanDP.html, where they are freely available, with more detailed references provided in the figure captions. Figures 1, 2, 5, and 7-17, Supplementary Figures 1 and 2, and Supplementary Tables 1 and 2 constitute data that are original with this paper. When this manuscript is accepted, the tabulated data will uploaded to the Zenodo repository (https://zenodo.org).

8. References cited

Abers GA, MacKenzie LS, Rondenay S, Zhang Z, Wech AG, Creager KC. 2009. Imaging the source regionof Cascadia tremor and intermediate-depth earthquakes. *Geology* 37: 1119-22

Abers GA, Nakajima J, vanKeken PE, Kita S, Hacker BR. 2013. Thermal–petrological controls on the location of earthquakes within subducting plates. *Earth Planet Sci. Lett.* 369-370: 178-87

Abu-Jaber NS, Kimberley MM. 1992. Origin of ultramafic-hosted vein magnesite deposits. *Ore Geol. Reviews* 7: 155-91

Aftabi A, Zarrinkoub MH. 2013. Petrogeochemistry of listvenite association in metaophiolites of Sahlabad region, eastern Iran: Implications for possible epigenetic Cu–Au ore exploration in metaophiolites. *Lithos* 156: 186-203

Agard P, Yamato P, Soret M, Prigent C, Guillot S, Plunder A, Dubacq B, Chauvet A, Monié P. 2016. Plate interface rheological switches during subduction infancy: Control on slab penetration and metamorphic sole formation. *Earth Planet Sci. Lett.* 451: 208-20

Akbulut M, Piskin O, Karayigit AI. 2006. The genesis of the carbonatized and silicified ultramafics known as listvenites: A case study from the Mihaliccik region (Eskisehir), NW Turkey. *Geol. J.* 41: 557-80

Al Khirbash S. 2015. Genesis and mineralogical classification of Ni-laterites, Oman Mountains. *Ore Geol. Reviews* 65: 199-212

Alabaster T, Pearce JA, Malpas J. 1982. The volcanic stratigraphy and petrogenesis of the Oman ophiolite complex. *Contrib. Mineral. Petrol.* 81: 168-83

Allegre CJ, Montigny R, Bottinga Y. 1973. Cortège ophiolitique et cortège océanique, géochimie comparée et mode de genèse. *Bulletin de la Societé Géologique de France* 7

Alsharan AS, Nasir SJY. 1996. Sedimentological and geochemical interpretation of a transgressive sequence: the Late Cretaceous Oahlah Formation in the western Oman Mountains, United Arab Emirates. *Sedimentary Geol.* 101: 227-42

Amri I, Ceuleneer G, Benoit M, Python M, Puga E, Targuisti K. 2007. Genesis of granitoids by interaction between mantle peridotites and hydrothermal fluids in oceanic spreading setting in the Oman ophiolite. *GEOGACETA* 42: 23-6

Andreani M, Baronnet A, Boullier A-M, Gratier J-P. 2004. A microstructural study of a “crack-seal” type serpentine vein using SEM and TEM techniques. *Eur. J. Mineral.* 16: 585-95

Arisi Rota F, Brondi A, Dessau G, Branzini M, Stea B, Vighi L. 1971. I giacimenti minerari. In ‘‘La Toscana Meridionale. Fondamenti geologico-minerari per una prospettiva di valorizzazione delle risorse naturali’’. *Rendiconti S.I.M.P.* 27: 357-544

Asimow PD, Dixon JE, Langmuir CH. 2004. A hydrous melting and fractionation model for mid-ocean ridge basalts: Application to the Mid-Atlantic Ridge near the Azores. *G-cubed* 5

Bailey EH. 1981. Geologic map of Muscat-Ibra area, Sultanate of Oman. *J. Geophys. Res.* 86: pocket map

Barnes I, O'Neill JR, Rapp JB, White DE. 1973. Silica-carbonate alteration of serpentine: Wall rock alteration in mercury deposits of the California Coast Ranges. *Econ. Geol.* 68: 388-98

Béchennec F, Le Metour J, Rabu D, Bourdillon-de-Grissac C, De Wever P, Beurrier M, Villey M. 1990. The Hawasina Nappes: stratigraphy, palaeogeography and structural

evolution of a fragment of the south-Tethyan passive continental margin. *Geol. Soc. Special Pub.* 49: 213-23
Béchennec F, Le Métour J, Rabu D, Villey M, Beurrier M. 1988. The Hawasina Basin: A fragment of a starved passive continental margin, thrust over the Arabian Platform during obduction of the Sumail Nappe. *Tectonophys.* 151: 323-43
Beinlich A, Austrheim H, Glodny J, Erambert M, Andersen TB. 2010. CO2 sequestration and extreme Mg depletion in serpentinized peridotite clasts from the Devonian Solund basin, SW-Norway. *Geochim. Cosmochim. Acta* 74: 6935-64
Beinlich A, Plümper O, Boter E, Müller IA, Kourim F, Ziegler M, Harigane Y, Lafay R, Kelemen PB, Oman Drilling Project Science Team. 2020. Ultramafic rock carbonation: Constraints from listvenite core BT1B, Oman Drilling Project. *J. Geophys. Res.* 125: e2019JB019060
Benoit M, Ceuleneer G, Polvé M. 1999. The remelting of hydrothermally altered peridotite at mid-ocean ridges by intruding mantle diapirs. *Nature* 402: 514-8
Berman RG. 1988. Internally-consistent thermodynamic data for minerals in the system Na2O-K2O-CaO-MgO-FeO-Fe2O3-Al2O3-SiO2-TiO2-H2O-CO2. *J. Petrol.* 29: 445-522
Borojević Šoštarić S, Palinkaš AL, Neubauer F, Cvetković V, Bernroider M, Genser J. 2014. The origin and age of the metamorphic sole from the Rogozna Mts., Western Vardar Belt: New evidence for the one-ocean model for the Balkan ophiolites. *Lithos* 192: 39-55
Boschi C, Dini A, Dallai L, Ruggieri G, Gianelli G. 2009. Enhanced CO2-mineral sequestration by cyclic hydraulic fracturing and Si-rich fluid infiltration into serpentinites at Malentrata (Tuscany, Italy). *Chem. Geol.* 265: 209-26
Bottinga Y, Allegre CJ. 1973. Thermal aspects of sea-floor spreading and the nature of the oceanic crust. *Tectonophys.* 18: 1-17
Boudier F, Ceuleneer G, Nicolas A. 1988. Shear zones, thrusts and related magmatism in the Oman ophiolite: Initiation of thrusting on an oceanic ridge. *Tectonophys.* 151: 275-96
Boudier F, Coleman RG. 1981. Cross section through the peridotite in the Semail ophiolite. *J. Geophys. Res.* 86: 2573-92
Braun MG, Kelemen PB. 2002. Dunite distribution in the Oman ophiolite: Implications for melt flux through porous dunite conduits. *G-cubed* 3
Breton J-P, Béchennec F, Le Métour J, Moen-Maurel L, Razin P. 2004. Eoalpine (Cretaceous) evolution of the Oman Tethyan continental margin: insights from a structural field study in Jabal Akhdar (Oman Mountains). *GeoArabia* 9: 41-58
Briqueu L, Mével C, Boudier F. 1991. Sr, Nd and Pb isotopic constraints on the genesis of a calc-alkaline plutonic suite in the Oman mountains related to the obduction process. In *Ophiolite genesis and evolution of the oceanic lithosphere*, ed. T Peters, A Nicolas, RG Coleman, pp. 517-42. Muscat, Oman: Ministry of Petroleum and Minerals, Sultanate of Oman
Carmichael DM. 1987. Induced stress and secondary mass transfer: Thermodynamic basis for the tendency toward constant-volume constraint in diffusion metasomatism. In *Chemical Transport in Metasomatic Processes, NATO ASI Series C, 218.*, ed. HC Helgeson, pp. 239-64. Dordrecht: Springer
Chemenda AI, Burg J-P, Mattauer M. 2000. Evolutionary model of the Himalaya^Tibet system: Geopoem based on new modelling, geological and geophysical data. *Earth Planet Sci. Lett.* 174: 397-409

Christensen NL, Smewing JD. 1981. Geology and seismic structure of the sorthern section of the Oman Ophiolite. *J. Geophys. Res.*: 2545-55

Coleman RG, Hopson CA, eds. 1981. *Oman Ophiolite Special Issue, J. Geophys. Res.*, Vols. 86. 2495-782 pp.

Coleman RG, Keith TE. 1971. Chemical Study of Serpentinization - Burro Mountain, California. *Journal of Petrology* 12: 311-&

Connolly JAD. 1990. Multivariable phase-diagrams - an algorithm based on generalized thermodynamics. *Am. J. Sci.* 290: 666-718

Connolly JAD. 2005. Computation of phase equilibria by linear programming: A tool for geodynamic modeling and its application to subduction zone decarbonation. *Earth Planet Sci. Lett.* 236: 524-41

Connolly JAD. 2009. The geodynamic equation of state: what and how. *G-cubed* 10: Q10014 DOI:10.1029/2009GC002540

Cooper DJW. 1988. Structure and sequence of thrusting in deep-water sediments during ophiolite emplacement in the south-central Oman Mountains. *J. Struct. Geol.* 10: 473-85

Cowan RJ, Searle MP, Waters DJ. 2014. Structure of the metamorphic sole to the Oman Ophiolite, Sumeini Window and Wadi Tayyin: implications for ophiolite obduction processes. *Geol. Soc. London Spec. Pub.* 392: 155-75

Cox J, Searle M, Pedersen R. 1999. The petrogenesis of leucogranitic dykes intruding the northern Semail ophiolite, United Arab Emirates: field relationships, geochemistry and Sr/Nd isotope systematics. *Contrib. Mineral. Petrol* 137: 267-87

de Obeso JC, Kelemen PB. 2018. Fluid rock interactions in residual mantle peridotites overlain by shallow oceanic limestones: Insights from Wadi Fins, Sultanate of Oman. *Chem. Geol.* 498: 139-49

de Obeso JC, Kelemen PB, Leong JA, Menzel MD, Manning CE, Menzel MD, Godard M, Cai YM, Bolge L, Oman Drilling Project Phase 1 Science Party. 2021a. Deep sourced fluids for peridotite carbonation in the shallow mantle wedge of a fossil subduction zone. *J. Geophys. Res.* revised and in review, preprint available at https://www.essoar.org/doi/10.1002/essoar.10507483.1

de Obeso JC, Santiago Ramos D, Higgins J, Kelemen P. 2021b. A Mg isotopic perspective on the mobility of magnesium during serpentinization and carbonation of the Oman ophiolite. *J. Geophys. Res.* 126: e2020JB020237

Deines P. 2002. The carbon isotope geochemistry of mantle xenoliths. . *Earth-Science Rev.* 58: 247-78

Duncan RA. 1982. A captured island chain in the Coast Range of Oregon and Washington. *J. Geophys. Res.* 87: 10,827-10,37

Durney DW, Ramsay JG. 1973. Incremental strain measured by syntectonic crystallization growths. In *Gravity and Tectonics*, ed. KA De Jong, R Scholten, pp. 67-96. New York: John Wiley

Ece ÖI, Matsubaya O, Çoban F. 2005. Genesis of hydrothermal stockwork-type magnesite deposits associated with ophiolite complexes in the Kütahya-Eskişehir region, Turkey. *Neues Jahrbuch für Mineragie-Abhandlungen* 181: 191-205

Ernewein M, Pflumio C, Whitechurch H. 1988. The death of an accretion zone as evidenced by the magmatic history of the Sumail ophiolite (Oman). *Tectonophys.* 151: 247-74

Escayola MP, Proenza JA, van Staal C, Rogers N, Skulski T. 2009. The Point Rousse listvenites, Baie Verte, Newfoundland: Altered ultramafic rocks with potential for gold

mineralization? *Current Research, Newfoundland & Labrador Dept. of Natural Res.* 09-1: 1-12
Facq S, Daniel I, Montagnac G, Cardon H, Sverjensky DA. 2016. Carbon speciation in saline solutions in equilibrium with aragonite at high pressure. Chem. Geol. 431, 44–53. *Chem. Geol.* 431: 44-63
Falk ES. 2014. *Carbonation of Peridotite in The Oman Ophiolite*. Columbia University, New York, NY, USA. 233 pp.
Falk ES, Kelemen PB. 2015. Geochemistry and petrology of listvenite in the Oman Ophiolite: Complete carbonation of peridotite during ophiolite emplacement. *Geochim. Cosmochim. Acta* 160: 70-90
Fletcher RC, Merino E. 2001. Mineral growth in rocks: kinetic-rheological models of replacement, vein formation, and syntectonic crystallization. *Geochim. Cosmochim. Acta* 65: 3733-48
Foley SF, Fischer TP. 2017. An essential role for continental rifts and lithosphere in the deep carbon cycle. *Nature Geosci.* 10: 897-902
Francis GH. 1956. The serpentinite mass in Glen Urquhart, Inverness-shire, Scotland. *Am. J. Sci.* 254: 201-26
Garber JM, Rioux M, Kylander-Clark AR, Hacker BR, Vervoort JD, Searle MP. 2020. Petrochronology of Wadi Tayin metamorphic sole metasediment, with implications for the thermal and tectonic evolution of the Samail Ophiolite (Oman/UAE). *Tectonics* 39: e2020TC006135
Garcia del Real P, Maher K, Kluge T, Bird DK, Brown GE, John CM. 2016. Clumped-isotope thermometry of magnesium carbonates in ultramafic rocks. *Geochim. Cosmochim. Acta* 193: 222-50
Gerbert-Gaillard L. 2002. *Caractérisation Géochimique des Péridotites de l'ophiolite d'Oman : processus magmatiques aux limites lithosphère/asthenosphère*. Université Montpellier II - Sciences et Techniques du Languedoc, Montpellier, FR. 241 pp.
Ghent ED, Stout MZ. 1981. Metamorphism at the base of the Samail ophiolite, southeastern Oman mountains. *J. Geophys. Res.* 86: 2557-71
Glennie KW, Boeuf MGA, Hughes-Clark MW, Moody-Stuart M, Pilaar WFH, Reinhardt BM. 1974a. Geology of the Oman Mountains. *Verh. K. Ned. Geol. Mijnbouwk. Gen.* 31
Glennie KW, Boeuf MGA, Hughes-Clarke MW, Moody-Stuart M, Pilaar WFH, Reinhardt BM. 1973. Late Cretaceous nappes in the Oman Mountains and their geologic evolution. *Am. Assoc. Petroleum Geol. Bull.* 57: 5-27
Glennie KW, Boeuf MGA, Hughes-Clarke MW, Moody-Stuart M, Pilaar WFH, Reinhardt BM. 1974b. Geology of the Oman Mountains. *Kon. Nederlands Geol. Mijb. Gen. Ver. Verh.* 31: 1-423
Godard M, Carter EJ, Decrausaz T, Lafay R, Bennett E, Kourim F, Obeso J-Cd, Michibayashi K, Harris M, Coggon JA, Teagle DAH, Kelemen PB, Oman Drilling Project Phase 1 Science Party. 2021. Geochemical profiles across the listvenite-metamorphic transition in the basal megathrust of the Semail Ophiolite: Results from drilling at Oman DP Hole BT1B. *J. Geophys. Res.* in press
Godard M, Jousselin D, Bodinier J-L. 2000. Relationships between geochemistry and structure beneath a palaeo-spreading centre: A study of the mantle section in the Oman ophiolite. *Earth Planet. Sci. Lett.* 180: 133-48

Gottschalk M. 1997. Internally consistent thermodynamic data for rock-forming minerals in the system SiO2-TiO2-Al2O3-Fe2O3-CaO-MgO-FeO-K2O-Na2O-H2O-CO2. *Eur. J. Mineral.* 9: 175-223

Green DH. 1961. Ultramafic breccias from the Musa Valley, eastern Papua. *Geol. Mag.* 98: 1-26

Green DH. 1964. The petrogenesis of the high-temperature peridotite intrusion in the Lizard area, Cornwall. *J. Petrol.* 5: 134-88

Gregory RT, Taylor Jr HP. 1981. An oxygen isotope profile in a section of Cretaceous oceanic crust, Samail Ophiolite, Oman: Evidence for δ18O buffering of the oceans by deep (> 5 km) seawater-hydrothermal circulation at mid-ocean ridges. *J. Geophys. Res.* 86: 2737-55

Grobe A, Virgo S, von Hagke C, Urai JL, Littke R. 2018. Multiphase structural evolution of a continental margin during obduction orogeny: Insights from the Jebel Akhdar dome, Oman mountains. *Tectonics* 37: 888-913

Grobe A, von Hagke C, Littke R, Dunkl I, Wübbeler F, Muchez P, Urai JL. 2019. Tectono-thermal evolution of Oman's Mesozoic passive continental margin under the obducting Semail Ophiolite: a case study of Jebel Akhdar, Oman. *Solid Earth* 10: 149–75

Guilmette C, Smit MA, Hinsbergen DJJv, Gürer D, Corfu F, Charette B, Maffione M, Rabeau O, Savard D. 2018. Forced subduction initiation recorded in the sole and crust of the Semail Ophiolite of Oman. *Nature Geosci.* 11: 699-5

Haase KM, Freund S, Beier C, Koepke J, Erdmann M, Hauff F. 2016. Constraints on the magmatic evolution of the oceanic crust from plagiogranite intrusions in the Oman ophiolite. *Contrib. Mineral. Petrol* 171: 1-16

Haase KM, Freund S, Koepke J, Hauff F, Erdmann M. 2015. Melts of sediments in the mantle wedge of the Oman ophiolite. *Geology* 43: 275-8

Hacker BR. 1996. Eclogite formation and the rheology, buoyancy, seismicity, and H2O content of oceanic crust. *AGU Monograph* 96: 337-46

Hacker BR. 2006. Pressures and temperatures of ultrahigh-pressure metamorphism: Implications for UHP tectonics and H2O in subducting slabs. *Int. Geol. Rev.* 48: 1053–66

Hacker BR, Gnos E. 1997. The conundrum of Samail: Explaining the metamorphic history. *Tectonophys.* 279: 215-26

Hacker BR, Mosenfelder JL. 1996. Metamorphism and deformation along the emplacement thrust of the Samail ophiolite, Oman. *Earth Planet Sci. Lett.* 144: 435-51

Hacker BR, Mosenfelder JL, Gnos E. 1996. Rapid emplacement of the Oman ophiolite: thermal and geochronologic constraints. *Tectonics* 15: 1230-47

Halls C, Zhao R. 1995. Listvenite and related rocks: Perspectives on terminology and mineralogy with reference to an occurrence at Cregganbaun, Co. Mayo, Republic of Ireland. *Mineral. Deposita* 30: 303-13

Hanghoj K, Kelemen PB, Hassler D, Godard M. 2010. Composition and genesis of depleted mantle peridotites from the Wadi Tayin massif, Oman ophiolite; Major and trace element geochemistry, and Os isotope and PGE systematics. *J. Petrol.* 51: 201-27

Hansen LD, Dipple GM, Gordon TM, Kellett DA. 2005. Carbonated serpentinite (listwanite) at Atlin, British Columbia: A geological analogue to carbon dioxide sequestration. *Can. Mineral.* 43: 225-39

Hansman RJ, Ring U, Thomson SN, den Brok B, Stübner K. 2017a. Late Eocene uplift of the Al Hajar Mountains, Oman, supported by stratigraphy and low-temperature thermochronology. *Tectonics* 36: 3081-109

Hansman RJ, Ring U, Thomson SN, den Brok B, Stübner K. 2017b. Late Eocene uplift of the Al Hajar Mountains, Oman, supported by stratigraphy and low-temperature thermochronology. *Tectonics* 36: 3081–109

Helgeson HC. 1985. Errata II. Thermodynamics of minerals, reactions, and aqueous solutions at high pressures and temperature. *Am. J. Sci.* 285: 8450855

Helgeson HC, Delany JM, Nesbitt HW, Bird DK. 1978. Summary and critique of the thermodynamic properties of rock-forming minerals. *Am. J. Sci.* 278-A: 1-229

Helgeson HC, Kirkham DH, Flowers GC. 1981. Theoretical prediction of the thermodynamic behavior of aqueous electrolytes by high pressures and temperatures; IV, Calculation of activity coefficients, osmotic coefficients, and apparent molal and standard and relative partial molal properties to 600 degrees C and 5kb. *Am. J. Sci.* 281: 1249-516

Herwegh M, Mercolli I, Linckens J, Müntener O. 2016. Mechanical anisotropy controls strain localization in upper mantle shear zones. *Tectonics* 35: 1177-204

Hirose F, Nakajima J, Hasegawa A. 2008. Three-dimensional seismic velocity structure and configuration of the Philippine Sea slab in southwestern Japan estimated by double-difference tomography. *J. Geophys. Res.* 113: http://dx.doi.org/10.1029/2007JB005274

Holland T, Powell R. 2003. Activity–composition relations for phases in petrological calculations: an asymmetric multicomponent formulation. *Contrib. Mineral. Petrol* 145: 492-501

Holland TJB, Powell RTJB. 1998. An internally consistent thermodynamic data set for phases of petrological interest. *J. Metamorphic Geol.* 16: 309-43

Horita J. 2014. Oxygen and carbon isotope fractionation in the system dolomite–water–CO2 to elevated temperatures. *Geochim. Cosmochim. Acta* 129: 11-124

Huang F, Sverjensky DA. 2019. Extended Deep Earth Water Model for predicting major element mantle metasomatism. *Geochim. Cosmochim. Acta* 254: 192-230

Ishikawa T, Nagaishi K, Umino S. 2002. Boninitic volcanism in the Oman ophiolite: Implications for thermal condition during transition from spreading ridge to arc. *Geology* 30: 899-902

Jamtveit B, Putnis C, Malthe-Sorenssen A. 2009. Reaction induced fracturing during replacement processes. *Contrib. Mineral. Petrol.* 157: 127-33

Johnson JW, Oelkers EH, Helgeson HC. 1992. SUPCRT92 - A software package for calculating the standard molal thermodynamic properties of minerals, gases, aqueous species, and reactions from 1-bar to 5000-bar and 0C to 1000C. *Computers and Geosciences* 18: 899-947

Jurković I, Palinkaš LA, Garašić V, Strmić Palinkaš S. 2012. Genesis of vein-stockwork cryptocrystalline magnesite from the Dinaride ophiolites. *Ophioliti* 37: 13-26

Kelemen PB, Braun M, Hirth G. 2000. Spatial distribution of melt conduits in the mantle beneath oceanic spreading ridges: Observations from the Ingalls and Oman ophiolites. *G-cubed* 1: doi:10.1029/999GC000012

Kelemen PB, Evans O, Ghiorso M, Mustard J, Ehlmann BL, Spiegelman M. 2020a. Carbonate in Olivine-Rich Unit (s) on Mars May Have Formed at Low P (H2O). *Lunar & Planetary Science Conference Abstracts*: 1213

Kelemen PB, Hirth G. 2012. Reaction-driven cracking during retrograde metamorphism: Olivine hydration and carbonation. *Earth Planet. Sci. Lett.* 345-348: 81–9

Kelemen PB, Koga K, Shimizu N. 1997. Geochemistry of gabbro sills in the crust-mantle transition zone of the Oman ophiolite: Implications for the origin of the oceanic lower crust. *Earth Planet. Sci. Lett.* 146: 475-88

Kelemen PB, Leong JA, de Obeso JC, Matter JM, Ellison ET, Templeton A, Nothaft DB, Eslami A, Evans KA, Godard M, Malvoisin B, Coggon JA, Warsi NH, Pézard P, Choe S, Teagle DAH, Michibayashi K, Takazawa E, Al Sulaimani Z, Team ODPS. 2021. Initial results from the Oman Drilling Project Multi-Borehole Observatory: Petrogenesis and ongoing alteration of mantle peridotite in the weathering horizon

Peter B. Kelemen1, James A. Leong1, Juan Carlos de Obeso2, Jürg M. Matter3, Eric T. Ellison4, Alexis Templeton4, Daniel B. Nothaft5, Alireza Eslami6, Katy Evans7, Marguerite Godard8, Benjamin Malvoisin9, Jude A. Coggon3, Nehal H. Warsi10, Philippe Pézard8, Saebyul Choe11, Damon A.H. Teagle3, Katsuyoshi Michibayashi12, Eiichi Takazawa13, Zaher Al Sulaimani14 and the Oman Drilling Project Science Team. *J. Geophys. Res.*: accepted

Kelemen PB, Manning CE. 2015. Reevaluating carbon fluxes in subduction zones: What goes down, mostly comes up. *Proc. Nat. Acad. Sci.* 112: E3997-E4006. https://doi.org/10.1073/pnas.1507889112

Kelemen PB, Matter JM, Teagle DAH, Coggon JA, Oman Drilling Project Science Team. 2020b. Site BT1: fluid and mass exchange on a subduction zone plate boundary, http://publications.iodp.org/other/Oman/VOLUME/CHAPTERS/113_BT1.PDF. In *Proceedings of the Oman Drilling Project, http://publications.iodp.org/other/Oman/OmanDP.html*, ed. PB Kelemen, JM Matter, DAH Teagle, JA Coggon, Oman Drilling Project Science Team. College Station, TX: International Ocean Discovery Program

Kelemen PB, Matter JM, Teagle DAH, Coggon JA, Team ODPS. 2020c. *Proceedings of the Oman Drilling Project, doi:10.14379/Oman.ph1-2.proc.2020.* College Station, TX: International Ocean Discovery Program

Kelemen PB, Shimizu N, Salters VJM. 1995. Extraction of mid-ocean-ridge basalt from the upwelling mantle by focused flow of melt in dunite channels. *Nature* 375: 747-53

Kerrick DM, Connolly JAD. 2001. Metamorphic devolatilization of subducted oceanic metabasalts: Implications for seismicity, arc magmatism and volatile recycling. *Earth Planet Sci. Lett.* 189

Kerrick DM, Jacobs GK. 1981. A modified Redlich-Kwong equation for H2O, CO2, and H2O-CO2 mixtures at elevated pressures and temperatures. *Am. J. Sci.* 281: 735-67

Khedr MZ, Arai S, Python M. 2013. Petrology and chemistry of basal lherzolites above the metamorphic sole from Wadi Sarami central Oman ophiolite. *J. Mineral. Petrol. Sci.* 108: 13-24

Khedr MZ, Arai S, Python M, Tamura A. 2014. Chemical variations of abyssal peridotites in the central Oman ophiolite: Evidence of oceanic mantle heterogeneity. *Gondwana Res.* 25: 1242-62

Klein EM, Langmuir CH. 1987. Global correlations of ocean ridge basalt chemistry with axial depth and crustal thickness. *J. Geophys. Res.* 92: 8089-115

Klein F, Garrido C-J. 2011. Thermodynamic constraints on mineral carbonation of serpentinized peridotite. *Lithos* 126: 147-60

Klein F, Le Roux V. 2020. Quantifying the volume increase and chemical exchange during serpentinization. *Geology* 48: 552-6

Kotowski A, Cloos M, Stockli D, Orent EB. 2021. Structural and thermal evolution of an infant subduction shear zone: Insights from sub-ophiolite metamorphic rocks recovered from Oman Drilling Project Site BT-1B. *J. Geophys. Res.* revised and in review, preprint available online at https://www.essoar.org/doi/10.1002/essoar.10505943.1

Lacinska AM, Styles MT. 2013. Silicified serpentinite–a residuum of a Tertiary palaeo-weathering surface in the United Arab Emirates. *Geol. Mag.* 150: 385-95

Lanphere MA, Coleman RG, Hopson CA. 1981. Sr isotopic tracer study of the Samail ophiolite, Oman. *J. Geophys. Res.* 86: 2709-20

Lapham DM. 1961. New data on deweylite. *Am. Min.* 46: 168-88

Li S-G, Yang W, Ke S, Meng X, Tian H, Xu L, He Y, Huang J, Wang X-C, Xia Q, Sun W, Yang X, Ren Z-Y, Wei H, Liu Y, Meng F, Yan J. 2017. Deep carbon cycles constrained by a large-scale mantle Mg isotope anomaly in eastern China. *National Science Review* 4: 111-20

Linckens J, Herwegh M, Müntener O, Mercolli I. 2011. Evolution of a polymineralic mantle shear zone and the role of second phases in the localization of deformation. *J. Geophys. Res.* 116: B06210

Lippard SJ, Shelton AW, Gass IG. 1986. *The Ophiolite of Northern Oman. Geological Society London Memoir 11*. 178 pp.

MacLeod CJ, Lissenberg CJ, Bibby LE. 2013. "Moist MORB" axial magmatism in the Oman ophiolite: the evidence against a mid-ocean ridge origin. *Geology* 41: 459-62

Malvoisin B. 2015. Mass transfer in the oceanic lithosphere: serpentinization is not isochemical. *Earth Planet Sci. Lett.* 430: 75-85

Malvoisin B, Zhang C, Müntener O, Baumgartner LP, Kelemen PB, Oman Drilling Project Science Team. 2020. Measurement of volume change and mass transfer during serpentinisation: Insights from the Oman Drilling Project. *J. Geophys. Res.* 125: e2019JB018877

McCulloch MT, Gregory RT, Wasserburg GJ, Taylor Jr HP. 1980. A neodymium, strontium, and oxygen isotopic study of the Cretaceous Samail Ophiolite and implications for the petrogenesis and seawater-hydrothermal alteration of oceanic crust. *Earth Planet Sci. Lett.* 46: 201-11

McCulloch MT, Gregory RT, Wasserburg GJ, Taylor Jr HP. 1981. Sm-Nd, Rb-Sr, and 18O/16O isotopic systematics in an oceanic crustal section: Evidence from the Samail Ophiolite. *J. Geophys. Res.* 86: 2721-35

McKenzie D, Bickle MJ. 1988. The volume and composition of melt generated by extension of the lithosphere. *J. Petrol.* 29: 625-79

Menzel MD, Garrido CJ, López Sánchez-Vizcaíno V, Marchesi C, Hidas K, Escayola MP, Delgado Huertas A. 2018. Carbonation of mantle peridotite by CO2-rich fluids: the formation of listvenites in the Advocate ophiolite complex (Newfoundland, Canada). *Lithos* 323: 238-61

Menzel MD, Urai JL, Obeso JCd, Kotowski A, Manning CE, Kelemen PB, Kettermann M, Jesus AP, Harigane Y, Team ODPPS. 2020. Brittle deformation of carbonated peridotite: Insights from listvenites of the Samail Ophiolite (Oman Drilling Project Hole BT1B). *J. Geophys. Res.* 125: e2020JB020199

Menzel MD, Urai JL, Ukar E, Hirth G, Schwedt A, Kovács A, Kibkalo L, Kelemen PB. 2021. Ductile deformation during carbonation of serpentinized peridotite. *Nature*

Communications revised and in review, preprint available at https://eartharxiv.org/repository/object/2416/download/4961/

Monnier C, Girardeau J, Le Mée L, M. P. 2006. Along-ridge petrological segmentation of the mantle in the Oman ophiolite. *G-cubed* 7: doi:10.1029/2006GC001320

Nahon D, Merino E. 1987. Pseudomorphic replacement in tropical weathering: Evidence, geochemical consequences, and kinetic-rheological origin. *Am. J. Sci.* 297: 393-417

Nasir S, Al Sayigh A, Al Harthy A, Al-Khirbash S, Al-Jaaidi O, Musllam A, Al-Mishwat A, Al-Bu'saidi S. 2007. Mineralogical and geochemical characterization of listwaenite from the Semail Ophiolite, Oman. *Chemie der Erde* 67: 213-28

Nicolas A, Boudier F, Ildefonse B. 1996. Variable crustal thickness in the Oman ophiolite: Implication for oceanic crust. *J. Geophys. Res.* 101: 17,941-17,50

Nicolas A, Boudier F, Ildefonse B, Ball E. 2000. Accretion of Oman and United Arab Emirates ophiolite: Discussion of a new structural map. *Marine Geophys. Res.* 21: 147-79

Ninkabou D, Agard P, et al. 2021. Structure of the offshore obducted Oman margin: Emplacement of the Semail ophiolite and role of tectonic inheritance. *J. Geophys. Res.* in press

Nolan SC, Skelton PW, Clissold BP, Smewing JD. 1990. Maastrichtian to early Tertiary stratigraphy and palaeogeography of the Central and Northern Oman Mountains *Geol. Soc. Special Pub.* 49: 495-519

Okazaki K, Michibayashi K, Hatakeyama K, Abe N, Johnson K, Kelemen P. 2021. Major mineral fraction and physical properties of carbonated peridotite (listvenite) from ICDP Oman Drilling Project Hole BT1B inferred from X-ray CT core images *J. Geophys. Res.* in press

Oskierski HC, Bailey JG, Kennedy EM, Jacobsen G, Ashley PM, Dlugogorski BZ. 2013a. Formation of weathering-derived magnesite deposits in the New England Orogen, New South Wales, Australia: Implications from mineralogy, geochemistry and genesis of the Attunga magnesite deposit. *Mineralium Deposita* 48: 525-641

Oskierski HC, Dlugogorski BZ, Jacobsen G. 2013b. Sequestration of atmospheric CO2 in a weathering-derived, serpentinite-hosted magnesite deposit: 14C tracing of carbon sources and age constraints for a refined genetic model. *Geochim. Cosmochim. Acta* 122: 226-46

Pan D, Spanu L, Harrison B, Sverjensky DA, Galli G. 2013. Dielectric properties of water under extreme conditions and transport of carbonates in the deep Earth. *Proc. Nat. Acad. Sci.* 110: 6646–50

Peacock SM. 1996. Thermal and petrologic structure of subduction zones. *AGU Monograph* 96: 119-33

Peacock SM, van Keken PE, Holloway SD, Hacker BR, Abers GA, Fergason RL. 2005. Thermal structure of the Costa Rica – Nicaragua subduction zone. *Phys. Earth Planet. Int.* 149: 187-200

Pearce JA, Alabaster T, Shelton AW, Searle MP. 1981. The Oman Ophiolite as a Cretaceous Arc-Basin Complex: Evidence and Implications. *Phil. Trans. Roy. Soc. London* A300: 299-317

Pearce JA, Peate DW. 1995. Tectonic implications of the composition of volcanic arc magmas. *Ann. Rev. Earth Planet. Sci.* 23: 251-86

Penniston-Dorland SC, Kohn MJ, Manning CE. 2015. The global range of subduction zone thermal structures from exhumed blueschists and eclogites: Rocks are hotter than models. *Earth Planet Sci. Lett.* 428: 243-54

Posukhova TV, Panasian LL, Sas IE. 2013. Serpentinites of the ural: mineralogical features, petrophysical properties and subduction processes. *Open J. Geology*: doi:10.4236/ojg.2013

Powell R, Holland TJBH, Worley B. 1998. Calculating phase diagrams involving solid solutions via non-linear equations, with examples using THERMOCALC. *J. Metamorphic Geol.* 16: 577-88

Prigent C, Agard P, Guillot S, Godard M, Dubacq B. 2018a. Mantle wedge (de)formation during subduction infancy: Evidence from the base of the Semail ophiolitic mantle. *J. Petrol.* 59: 2061-92

Prigent C, Guillot S, Agard P, Lemarchand D, Soret M, Ulrich M. 2018b. Transfer of subduction fluids into the deforming mantle wedge during nascent subduction: Evidence from trace elements and boron isotopes (Semail ophiolite, Oman). *Earth Planet Sci. Lett.* 484: 213-28

Quesnel B, Boulvais P, Gautier P, Cathelineau M, John CM, Dierick M, Agrinier P, Drouillet M. 2016. Paired stable isotopes (O, C) and clumped isotope thermometry of magnesite and silica veins in the New Caledonia Peridotite Nappe. *Geochim. Cosmochim. Acta* 183: 234-49

Quesnel B, Gautier P, Boulvais P, Cathelineau M, Maurizot P, Cluzel D, Ulrich M, Guillot S, Lesimple S, Couteau C. 2013. Syn-tectonic, meteoric water–derived carbonation of the New Caledonia peridotite nappe. *Geology* 41: 1063-6

Raleigh CB, Paterson MS. 1965. Experimental deformation of serpentinite and its tectonic implications. *J. Geophys. Res.* 70: 3965-85

Reiners PW, Spell TL, Nicolescu S, Zanetti KA. 2004. Zircon (U-Th)/He thermochronometry: He diffusion and comparisons with 40Ar/39Ar dating. *Geochim. Cosmochim. Acta*: 1857-87

Rioux M, Benoit M, Amri I, Ceuleneer G, Garber JM, Searle M, Leal K. 2021a. The origin of felsic intrusions within the mantle section of the Samail ophiolite: Geochemical evidence for three distinct mixing and fractionation trends. *J. Geophys. Res.*: e2020JB020760

Rioux M, Bowring S, Kelemen P, Gordon S, Dudás F, Miller R. 2012. Rapid crustal accretion and magma assimilation in the Oman-U.A.E. ophiolite: High precision U-Pb zircon geochronology of the gabbroic crust. *J. Geophys. Res.* 117: B07201, doi:10.1029/2012JB009273

Rioux M, Bowring S, Kelemen P, Gordon S, Miller R, Dudás F. 2013. Tectonic development of the Samail ophiolite: High precision U-Pb zircon geochronology of crustal growth and ophiolite emplacement. *J. Geophys. Res.* 118: 2085-101

Rioux M, Garber J, Bauer A, Bowring S, Searle M, Kelemen P, Hacker B. 2016. Synchronous formation of the metamorphic sole and igneous crust of the Semail ophiolite: New constraints on the tectonic evolution during ophiolite formation from high-precision U-Pb zircon geochronology. *Earth Planet. Sci. Lett.* 451: 185-95

Rioux M, Garber J, Searle M, Kelemen P, Miyashita S, Adachi Y, Bowring S. 2021b. High-precision U-Pb zircon dating of late magmatic series in the Samail ophiolite: A record of subduction initiation. *J. Geophys. Res.* in press

Rollinson H. 2015. Slab and sediment melting during subduction initiation: granitoid dykes from the mantle section of the Oman ophiolite. *Contrib. Mineral. Petrol* 170: 1-20

Rudge JF, Kelemen PB, Spiegelman M. 2010. A simple model of reaction-induced cracking applied to serpentinization and carbonation of peridotite. *Earth Planet Sci. Lett.* 291: 215-27

Scambelluri M, Bebout GE, Belmonte D, Gilio M, Campomenosi N, Collins N, Crispini L. 2016. Carbonation of subduction-zone serpentinite (high-pressure ophicarbonate; Ligurian Western Alps) and implications for the deep carbon cycling. *Earth Planet Sci. Lett.* 441: 155-66

Scarsi M, Malatesta C, Fornasaro S. 2018. Lawsonite-bearing eclogite from a tectonic mélange in the Ligurian Alps: New constraints for the subduction plate-interface evolution. *Geol. Mag.* 155: 280-97

Scharf A, Mattern F, Bolhar R, Bailey CM, Ring U. 2020. *U-Pb dating of postobductional carbonate veins in listwaenite of the Oman Mountains near Fanja*. Presented at Proceedings of the International Conference on Ophiolites and the Oceanic Lithosphere: Results of the Oman Drilling Project and Related Research, Sultan Qaboos University, Oman

Schlüter M, Steuber T, Parente M, Mutterlose J. 2008. Evolution of a Maastrichtian–Paleocene tropical shallow-water carbonate platform (Qalhat, NE Oman). *Facies* 54: 513-27

Searle M, Cox J. 1999. Tectonic setting, origin, and obduction of the Oman ophiolite. *GSA Bull.* 111: 104-22

Searle M, Cox J. 2002. Subduction zone metamorphism during formation and emplacement of the Semail ophiolite in the Oman Mountains. *Geol. Mag.* 139: 241-55

Searle MP, Lippard SJ, Smewing JD, Rex DC. 1980. Volcanic rocks beneath the Semail Ophiolite nappe in the northern Oman mountains and their significance in the Mesozoic evolution of Tethys. *J. Geol. Soc. London* 137: 589-604

Searle MP, Malpas J. 1980. The structure and metamorphism of rocks beneath the Semail ophiolite of Oman and their significance in ophiolite obduction. *Trans. Roy. Soc. Edinburgh Earth Sci.* 71: 247-62

Searle MP, Malpas J. 1982. Petrochemistry and origin of sub-ophiolitic metamorphic and related rocks in the Oman Mountains. *J. Geol. Soc. London* 139: 235-48

Searle MP, Robertson AHF. 1990. The northern Oman Tethyan continental margin: Stratigraphy, structure, concepts and controversies. *Geol. Soc. Special Pub.* 49: 3-25

Searston SM. 1998. *Resource estimation and the Kunwarara magnesite deposit*. University of Tasmania, Hobart, Tasmania. 356 pp.

Shock EL, Oelkers EH, Johnson JW, Sverjensky DA, Helgeson HC. 1992. (1992) Calculation of the thermodynamic properties of aqueous species at high pressures and temperatures: Effective electrostatic radii, dissociation constants and standard partial molal properties to 1000 ————————————C and 5 kbar. *J. Chem. Soc. Faraday Trans.* 88: 803-26

Shock EL, Sassani DC, Willis M, Sverjensky DA. 1997. Inorganic species in geologic fluids: correlations among standard molal thermodynamic properties of aqueous ions and hydroxide complexes. *Geochim. Cosmochim. Acta* 61: 907-50

Sofiya A, Ishiwatari A, Hirano N, Tsujimori T. 2017. Relict chromian spinels in Tulu Dimtu serpentinites and listvenite, Western Ethiopia: implications for the timing of listvenite formation. *Int. Geol. Rev.* 59: 1621-31

Soret M, Agard P, Dubacq B, Plunder A, Yamato P. 2017. Petrological evidence for stepwise accretion of metamorphic soles during subduction infancy (Semail ophiolite, Oman and UAE). *J. Metamorphic Geol.* 35: 1051-80

Spencer CJ, Cavosie AJ, Raub TD, Rollinson H, Jeon H, Searle MP, Miller JA, McDonald BJ, Evans NJ. 2017. Evidence for melting mud in Earth's mantle from extreme oxygen isotope signatures in zircon. *Geology* 45: 975-8

Stanger G. 1985. Silicified serpentinite in the Semail nappe of Oman. *Lithos* 18: 13-22

Stewart EM, Ague JJ. 2020. Pervasive subduction zone devolatilization recycles CO2 into the forearc. *Nature Communications* 11: 1-8

Styles MT, Ellison RA, Phillips ER, Arkley S, Schofield DI, Thomas RJ, Goodenough KM, Farrant AR, McKervey JA, Crowley QG, Pharaoh TC. 2006. *The Geology and Geophysics of the United Arab Emirates, vol.2*. Abu Dhabi: Ministry of Energy, United Arab Emirates

Sverjensky DA, Harrison B, Azzolini D. 2014. Water in the deep Earth: the dielectric constant and the solubilities of quartz and corundum to 60 kb and 1200 C. *Geochim. Cosmochim. Acta* 129: 125-45

Syracuse EM, Keken PEv, Abers GA. 2010. The global range of subduction zone thermal models. *Phys. Earth Planet. Int.* 183: 73-90

Takazawa E, Okayasu T, Satoh K. 2003. Geochemistry and origin of the basal lherzolites from the northern Oman ophiolite (northern Fizh block). *G-cubed* 4: 1021

Tilton GR, Hopson CA, Wright JE. 1981. Uranium-lead isotopic ages of the Samail ophiolite, Oman, with applications to Tethyan ocean ridge tectonics. *J. Geophys. Res.* 86: 2736-75

Ulrich M, Munoz M, Guillot S, Cathelineau M, Picard C, Quesnel B, Boulvais P, Couteau C. 2014. Dissolution–precipitation processes governing the carbonation and silicification of the serpentinite sole of the New Caledonia ophiolite. *Contrib. Mineral. Petrol* 167: 952; doi 10.1007/s00410-013-0952-8

Urai JL, Williams PF, van Roermund HLM. 1991. Kinematics of crystal growth in syntectonic fibrous veins. *J. Struct. Geol.* 13: 823-36

van Hinsbergen DJJ, Maffione M, Koornneef LMT, Guilmette C. 2019. Kinematic and paleomagnetic restoration of the Semail ophiolite (Oman) reveals subduction initiation along an ancient Neotethyan fracture zone. *Earth Planet Sci. Lett.* 518: 183-96

van Keken PE, Wada I, Sime N, Abers GA. 2019. Thermal structure of the forearc in subduction zones: A comparison of methodologies. *G-cubed* 20: 3268–88

Villey M, Le Metour J, De Gramont X. 1986. *Geological Map of Fanjah. Muscat, Oman*. Muscat, Oman: Ministry of Petroleum and Minerals, Directorate General of Minerals, Sultanate of Oman

Warren C, Parrish R, Waters D, Searle M. 2005. Dating the geologic history of Oman's Semail ophiolite: insights from U–Pb geochronology. *Contrib. Mineral. Petrol.* 150: 403-22

Weyhenmeyer CE. 2000. *Origin and evolution of groundwater in the alluvial aquifer of the Eastern Batinah Coastal Plain, Sultanate of Oman : a hydrogeochemical approach*. University of Bern, Bern, CH

Wilde A, Simpson L, Hanna S. 2002. Preliminary study of Tertiary hydrothermal alteration and platinum deposition in the Oman ophiolite. *J. Virtual Explorer* 6: 7-13

Wilson CR, Spiegelman M, van Keken PE, Hacker BR. 2014. Fluid flow in subduction zones: The role of solid rheology and compaction pressure. *Earth Planet Sci. Lett.* 401: 261-74

Wohlwend S, Celestino R, Reháková D, Huck S, Weissert H. 2017. Late Jurassic to Cretaceous evolution of the eastern Tethyan Hawasina Basin (Oman Mountains). *Sedimentology* 64: 87-110

Wolery TJ. 1992. EQ3/6, a software package for geochemical modeling of aqueous systems: package overview and installation guide (version 7.0) (No. UCRL-MA--110662-PT. 1). *Lawrence Livermore National Lab*

Wyns R, Bechennec F, Le Meteour J, Roger J. 1992. Geological Map of the Tiwi Quadrangle, Sultanate of Oman. Geoscience Map, Scale 1:100,000, Sheet NF 40-8B. Muscat, Oman: Ministry of Petroleum and Minerals, Directorate General of Minerals, Sultanate of Oman

Yoshikawa M, Python M, Tamura A, Arai S, Takazawa E, Shibata T, Ueda A, Sato T. 2015. Melt extraction and metasomatism recorded in basal peridotites above the metamorphic sole of the northern Fizh massif, Oman ophiolite. *Tectonophys.* 650: 53-64

Zarrinkoub MH, Amini S, Aftabi A, Karimpour MH. 2005. Mineralogy, geochemistry, structural position and a genetic model for listvenite in the east of Iran. *Iranian J. Crystallography & Mineralogy* 13: 363-78

Zimmer K, Zhang YL, Lu P, ChenY.Y.., Zhang GR, Dalkilic M, Zhu C. 2016. SUPCRTBL: A revised and extended thermodynamic dataset and software package of SUPCRT92. *Computers and Geosciences* 90: 97-111